

Review

Polarised Raman spectroscopy for the study of molecular orientation distributions in polymers

M. TANAKA, R. J. YOUNG*

Materials Science Centre, School of Materials, University of Manchester, Grosvenor Street, Manchester, M1 7HS, UK

E-mail: robert.young@manchester.ac.uk

Polarised Raman spectroscopy is a vibrational spectroscopic technique that is used widely for the chemical and physical analyses of materials since it is both non-destructive and suitable for remote analysis. In particular over the last 40 years, the technique has been developed and applied for the study of molecular orientation distributions in polymers. Compared to other analytical techniques, polarised Raman spectroscopy has the following advantages, (1) quantitative and precise measurement of molecular orientation distributions, and (2) study of these distributions in both the crystalline and amorphous phases. Knowledge obtained from the technique is of both academic and industrial interest to study relationships between microstructure and macroscopic physical properties in polymers. In this paper, polarised Raman spectroscopy is reviewed with regard to the study of molecular orientation distributions in polymeric materials. The basis of polarised Raman scattering is first described, and this is followed by the procedure for obtaining spectra. It is shown how Raman scattering intensities for different polarised scattering geometries can be interpreted to give parameters and functions representing quantitative measures of the degree of molecular orientation. Factors affecting the evaluation of these parameters are also summarised. Finally, the usefulness of the technique is demonstrated by practical applications including a study of molecular orientation distributions in poly(ethylene terephthalate) (PET) fibres.

© 2006 Springer Science + Business Media, Inc.

1. Introduction

Macroscopic properties of materials are closely related to their microstructures. For semicrystalline polymers, the ratio of crystalline and amorphous phases, and molecular orientation in these phases are considered to be essential factors to understand this relationship and to optimise physical properties of the materials.

A number of techniques have been utilised for the study of the microstructures of polymeric materials. The crystallinity is regarded as a quantitative measure of the ratio of the crystalline and amorphous phases in the material, and obtained by relatively simple methods such as thermal analyses, density measurements and X-ray diffraction. On

the other hand, the molecular orientation in the materials has also been studied widely, although the majority of the studies have produced only qualitative information on molecular orientation.

Molecular orientation distribution functions, which show the distributions of molecules oriented with respect to a certain direction of the material, are considered as quantitative measures of molecular orientation in a material. These functions can be obtained by several techniques such as wide-angle X-ray diffraction (WAXD) [1–4], birefringence measurements [5–8], nuclear magnetic resonance (NMR) [9–12], and vibrational spectroscopic techniques. Each technique, however, has its advantages and

*Author to whom all correspondence should be addressed.

disadvantages. Birefringence measurements are simple and reasonable but give information [13, 14] only about the distributions averaged over the sample, while NMR is costly because it requires instruments with a high sensitivity for the purpose of the study. Molecular orientation distributions in the crystalline phases only are obtained [15–17] by WAXD, although this is only the technique allowing the precise distributions to be obtained, since all coefficients in the orientation distribution functions can be determined.

Focusing on the spectroscopic techniques, fluorescence spectroscopy [9, 18–20] provides information about the molecular orientation distributions in phases only where fluorescent probes can migrate. Infrared (IR) dichroism measurements [8, 21–23] are capable of evaluating the molecular orientation distributions in both the crystalline and amorphous phases. However, the distributions obtained by IR spectroscopy may lack accuracy since only one coefficient for the distribution functions can be determined [5–7]. Furthermore, the sample is required to be highly transparent and thin for the absorbance measurements. It is, therefore, normally necessary to combine these techniques to obtain information about the molecular orientation distributions in the crystalline and amorphous phases of the material.

Polarised Raman spectroscopy is a powerful tool to obtain information about molecular orientation distributions [7, 8, 24]. Similar to IR dichroism measurements, it is possible for this technique to analyse the distributions in both the crystalline and amorphous phases of the material simultaneously. Compared to IR spectroscopy, higher order coefficients for the distribution functions can be determined by means of polarised Raman spectroscopy. Therefore, a more detailed study about the molecular orientation distribution can be performed using polarised Raman spectroscopy. Since this technique is compatible with optical microscopy, polarised Raman spectroscopy is suitable for the study of molecular orientation distributions in the material at the micron size scale or in a micron region in the material. Furthermore, this technique has considerable potential for on-line monitoring of the quality of materials in production lines owing to its non-destructive nature and fast data acquisition.

First observed by Raman *et al.* in 1928 [25], Raman scattering can be described as the inelastic energy scattering of incident light, which has interacted with the polarisability of chemical bonds in a molecule. Due to a weak intensity of the scattering, Raman spectroscopy used to be regarded as a compensatory chemical analysis for Infrared (IR) spectroscopy in its early days. In latter decades, however, the technique has successfully extended its application fields, owing to the introduction of powerful monochromatic laser beams and charge-coupled device (CCD) detectors.

This paper will review the basis of Raman scattering, and its specific application for the study of molecular orientation distributions in polymers.

2. Theory of Raman scattering

2.1. Classical theory

Raman scattering is considered to be the inelastic energy scattering of light interacting with molecules [26, 27]. When incident light encounters a molecule, the electric field of the light induces a dipole moment in the molecule due to its polarisability. The amount of the induced dipole moment (μ) is given by,

$$\mu = \alpha E \quad (1)$$

where α is the molecular polarisability and E is the electric field of the incident light. Oscillation of the electric field, E , can be described as,

$$E = E_o \cos(2\pi\nu_o t) \quad (2)$$

where E_o is the amplitude of the oscillation, ν_o is the frequency of the incident light, and t is time.

Due to the oscillation of the electric field, the induced dipole moment of the molecule also oscillates. On the other hand, an oscillating dipole moment can absorb or emit energy by transitions between different oscillation energy levels [28]. This energy absorption process is used in IR spectroscopy, which monitors the energy transfer from photons of the incident light to molecules. Through this process the molecules are excited to their higher energy levels. Subsequently, the excited molecules go back to their lower energy levels by the emission of scattered light. This energy transition is usually energetically elastic, where the energy of the scattered photons has the same energy as those of the incident light, and is called *Rayleigh scattering*.

When the energy of the incident light is similar to the energy difference between different rotational or vibrational energy levels of molecules, however, the scattering process may involve energy transition of the excited molecules to a different energy level from their initial energy level. The scattering associated with this inelastic energy transition is called *Raman scattering*. Hereafter, Raman scattering is described in terms of the energy transition of molecules between their different vibrational energy levels, although the same theory is applicable to rotational energy transitions.

If a molecule is vibrating with a certain frequency, the displacement of the k -th atom in the molecule from its equilibrium position can be written by,

$$q_k = q_k^o \cos(2\pi\nu_m t) \quad (3)$$

where q_k^o is the amplitude of the displacement, and the term ν_m is the frequency of the vibration. The polarisability α of the molecule can be expanded in the form of Taylor series and expressed by,

$$\alpha = \alpha_o + \sum_k \left(\frac{\partial \alpha}{\partial q_k} \right)_{q_k=0} q_k + \frac{1}{2} \sum_{i,j} \left(\frac{\partial^2 \alpha}{\partial q_i \partial q_j} \right)_{q_i=q_j=0} q_i q_j + \dots \quad (4)$$

The displacement q_k concerning the molecular vibration is considered to be very small, and the high order terms (from the 3rd term in the right-hand side of the equation and above) can be neglected. The combination of Equations 1, 2 and 4 gives,

$$\begin{aligned} \mu &= \alpha_o E_o \cos(2\pi \nu_o t) \\ &+ \sum_k \left(\frac{\partial \alpha}{\partial q_k} \right)_{q_k=0} q_k E_o \cos(2\pi \nu_o t) \cos(2\pi \nu_m t) \\ &= \alpha_o E_o \cos(2\pi \nu_o t) \\ &+ \frac{1}{2} \sum_k \left(\frac{\partial \alpha}{\partial q_k} \right)_{q_k=0} q_k E_o \{ \cos[2\pi(\nu_o - \nu_m)t] \\ &+ \cos[2\pi(\nu_o + \nu_m)t] \} \end{aligned} \quad (5)$$

In Equation 5, the first and second terms are related to the Rayleigh scattering and Raman scattering, respectively. In the second term, the part containing $(\nu_o - \nu_m)$ is related to the Raman scattering for which the vibrational energy of the molecule moves to a higher energy level than its initial energy level (Stokes Raman scattering). In contrast, the scattering with the vibrational energy transition of the molecule from its initial energy level to a lower energy level (anti-Stokes Raman scattering) is related to the part with $(\nu_o + \nu_m)$.

From Equation 5, the condition for a vibrational mode to be Raman active is shown by,

$$\left(\frac{\partial \alpha}{\partial q_k} \right)_{q_k=0} \neq 0 \quad (6)$$

which indicates that the molecular polarisability of the vibrational mode should be neither maximum nor minimum when the atoms are at their equilibrium positions ($q_k = 0$).

2.2. Quantum mechanical approach

Although the classical theory of Raman scattering can be understood simply as shown in the previous section, some phenomena cannot be explained by the classical approach. For instance, the Stokes Raman scattering in-

tensity observed is usually higher than the corresponding anti-Stokes Raman scattering intensity. This observation would seem to be contradicting the rule in electromagnetic theory that the intensity of the light is proportional to the fourth power of its wavenumber (i.e., to the reciprocal fourth power of its wavelength) [29]. Such behaviour can be dealt with using a quantum mechanical approach.

In quantum mechanics, molecules can take [26, 27] discrete vibrational energy levels as shown in Fig. 1. The vibrational energy level (ε_v) for a harmonic oscillation can be described as a solution of Schrödinger equation by,

$$\varepsilon_v = \left(v + \frac{1}{2} \right) \nu_m \quad (7)$$

where v is a vibrational quantum number. Energy transitions of $\Delta v = 1, 2 \dots$ are allowed during Raman scattering. With respect to the probability of the transition, the transition with $\Delta v = 1$ has a much higher probability compared to other transitions, since the energy change as the result of the $\Delta v = 1$ transition is small.

In addition, molecules are likely to take the vibrational energy ε_v of their ground state ($v = 0$) in their initial state unless the temperature is very high. The population of the molecules with a vibrational energy ε_v is considered to follow the Maxwell-Boltzman distribution law. The Stokes and anti-Stokes Raman scattering intensities are correlated with the number of molecules making these transitions by,

$$\begin{aligned} \frac{I_{\text{Stokes}}}{I_{\text{anti-Stokes}}} &= \left(\frac{\nu_o - \nu_m}{\nu_o + \nu_m} \right)^4 \frac{N_v}{N_{v'}} \\ &= \left(\frac{\nu_o - \nu_m}{\nu_o + \nu_m} \right)^4 \exp \left(\frac{\varepsilon_v - \varepsilon_{v'}}{kT} \right) \end{aligned} \quad (8)$$

where ε_v and $\varepsilon_{v'}$ are the energy levels of the molecule before and after transition, respectively, and k and T are the Boltzman constant and temperature, respectively. At ambient temperature, therefore, the vibrational energy transition from $v = 0$ to $v = 1$ would be expected to occur with a high probability during Raman scattering, which explains the observation that the Stokes Raman scattering intensity is higher than the anti-Stokes Raman scattering intensity.

2.3. Applications of Raman spectroscopy

Similar to IR spectroscopy, Raman spectroscopy is a powerful tool for the analysis of chemical bonds in organic and inorganic materials [26, 30]. Since the vibrational energy (ν_m) is unique to the type of chemical bond in a molecule, it is useful for the analysis of molecular structure. The selection rules for Raman scattering activity also give several advantages over IR spectroscopy. Spectroscopic information can be obtained from the vibration

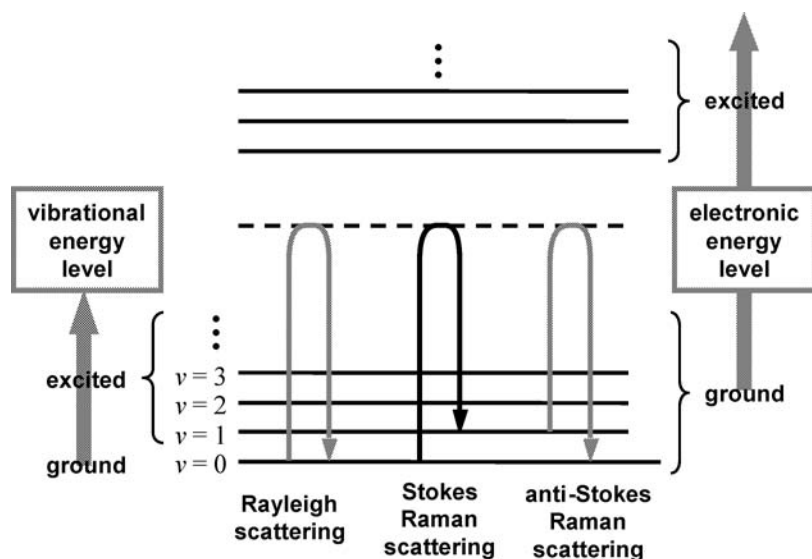


Figure 1 A schematic diagram for energy transitions during Rayleigh scattering, Stokes Raman scattering and anti-Stokes Raman scattering [26, 27].

of chemical bonds with small α_0 values but with large $(\frac{\partial\alpha}{\partial q_k})_{q_k=0}$ values such as stretching of a C–C bond. In contrast to IR spectroscopy, Raman spectra are much less affected by the presence of water in the samples, since an H₂O molecule has a large α_0 value but small $(\frac{\partial\alpha}{\partial q_k})_{q_k=0}$ values. Another advantage of Raman spectroscopy is that the Raman scattering intensity is related linearly to the number of chemical bonds in a sample, while the IR absorbance is related exponentially in accordance with Lambert-Beer's law. This leads to quantitative analyses by Raman spectroscopy being more straightforward than by IR spectroscopy.

Raman spectroscopy is also useful for the physical analysis of materials, since the value $(\frac{\partial\alpha}{\partial q_k})_{q_k=0}$ is sensitive to environments where the chemical bonds are located. Information that can be obtained by the technique includes molecular conformations and configurations, and morphologies such as the ordered and disordered phases in the materials. Furthermore, it is possible to collect Raman spectra from a micron-sized region of a sample when the technique is combined with optical microscopy. This enables Raman spectroscopy to analyse samples of the order of microns in size and the microstructure of a sample with micron-order resolution.

3. Applications of Raman scattering for the study of molecular orientation distributions in polymers

As described in the following sections, the differential polarisability of the molecular bond, $(\frac{\partial\alpha}{\partial q_k})_{q_k=0}$, is represented in the form of a second rank tensor, the so-called *Raman tensor*. Owing to the symmetry of the tensor, the Raman tensor is often illustrated as an

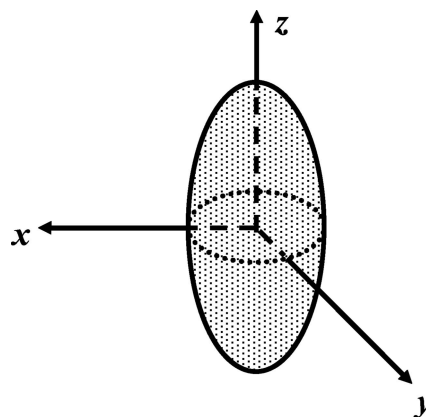


Figure 2 An ellipsoid for the representation of a Raman tensor.

ellipsoid shown in Fig. 2, where the shorter the axis of the ellipsoid, the larger the differential polarisability. Raman scattering is the interaction between the electric vector of incident light and the ellipsoid, and includes directional information about the ellipsoid. Furthermore, the shape of the ellipsoid and the orientation of the ellipsoids within the specimen can be determined precisely by the measurement of the angular distribution of the Raman scattering intensity by means of a monochromatic plane-polarised beam and an analyser. This enables the study of molecular orientation distributions in both the crystalline and non-crystalline phases of polymers.

3.1. Methodological development (chronology)

The concept of the Raman tensor for Raman spectroscopy was established first of all by Ovander [31] in 1960. His concept was based on molecular symmetry, and it

was further correlated with crystal structures by Loudon [32, 33] in 1964. To explain the three-dimensional distributions of the Raman tensor within a sample, Roe [9, 34] introduced spherical harmonics in 1965. On the other hand, in 1966 Porto [35] measured the polarisation direction dependence of the Raman scattering, termed as the *depolarisation ratio*, and related it with the Raman tensor. Scherer *et al.* [36] later in 1971 also measured the depolarisation ratio using a polarisation analyser. Although the change in Raman intensity using incident beam polarisation had already been observed by Raman *et al.* [37] in 1928, most of the theoretical understanding of the phenomenon was not achieved until the late 1960s.

The application of polarised Raman spectroscopy for the study of molecular orientation made great progress in the early 1970s. In 1971, Snyder [38] expressed successfully the correlation between the Raman tensor, molecular orientation and the observed intensity with the aid of the translation from molecular symmetry axes to sample symmetry axes. Bower [24] introduced in 1972 the idea of *molecular orientation distribution coefficients*, which are the coefficients that can be used to describe the orientation preference in materials, by means of polarised Raman spectroscopy. The coefficients can be associated with those obtained by the other techniques for the determination of molecular orientation distributions such as fluorescence spectroscopy and X-ray diffraction. He also provided a detailed explanation [39] about the relationship between the Raman tensor and the molecular orientation distribution coefficients in terms of molecular symmetry. The possible range of the molecular orientation distribution coefficients was also considered by Bower [40] in 1981, which agreed with the concept of Kawai and co-workers [2, 41] for X-ray and birefringence studies.

Orientation distribution coefficients are useful to express the degree of orientation in the sample. However, these coefficients can be correlated with the orientation direction averaged over the molecules of interest, and it is often meaningful to know the actual angular distributions of molecular orientation direction in terms of the *molecular orientation distribution functions*. In 1981, using numerical calculations based on the information entropy theory [42–44], Bower and co-workers [40, 45, 46] developed a method to depict the distribution as the so-called *most probable distribution curve* for a given set of orientation distribution coefficients.

These theoretical developments to obtain the molecular orientation distribution function were applied basically for the system in which the molecular symmetry axis is parallel to the chain backbone axis. However, some materials, poly(vinyl alcohol) and syndiotactic polypropylene for instance, possess their symmetry axes perpendicular to their chain axes. For such systems, a molecular orientation study can be undertaken by applying the geometrical calculations developed by Schlotter *et al.* [47] in 1984.

For the evaluation of the molecular orientation distribution coefficients, the most recent progress was reported by Nikolaeva and co-workers [48–50] in 1997. It is of great importance to normalise the Raman scattering intensity for different scattering geometries in order to determine the orientation coefficients, although the measurement can be influenced by the nature of the sample such as its birefringence. By comparing the intensity ratio of different Raman bands, their method could avoid the normalisation process, thus enabling the value of the orientation distribution function to be obtained in a simpler way.

3.2. Polarisation of Raman scattering

Light is an electromagnetic wave consisting of the vibration of an electric field and a magnetic field perpendicular to each other. In general, the light from a radiation source involves waves with no preferential direction of the electric field vector. When it encounters a substance, the light interferes with the atoms and induces a dipole moment in the material. The degree of the interference (induced dipole moment) depends on the angle between the electric vector of the incident light and the magnitude of the polarisability (Equation 1), and thus the differential polarisability. Thus, it may contain directional information about the orientation of the differential polarisability.

When light without a specified electric vector is used, however, it is difficult to obtain such information since its interference with molecules in the material can occur in any direction. On the other hand, the information can be obtained if polarised light with a specific electric vector is employed as the incident beam. In polarised Raman spectroscopy, the polarised Raman scattering is observed as a result of the interference of the polarised light with the molecules vibrating in the condition given by Equation 6. Furthermore, by means of an analyser, which is another polariser before the detector, the precise directional information about the differential polarisability of the molecules can be obtained; hence the orientation of the molecules can be determined.

Polarised Raman spectroscopy is also useful for vibrational mode assignments. Each vibrational mode possesses an individual differential polarisability ellipsoid, which determines the mode of the vibration. Depending on the shape of the ellipsoid, the Raman scattering intensity changes with the polarisation of the incident beam.

3.3. Depolarisation ratio

The measurement of the depolarisation ratio is of great importance to determine the shape of a differential polarisability ellipsoid and the orientation of the ellipsoid. The depolarisation ratio (ρ) is measured experimentally by,

$$\rho = \frac{I_{\perp}}{I_{\parallel}} \quad (9)$$

where, I_{\perp} and I_{\parallel} represent the Raman scattering intensities when the polarisation direction of analyser is normal and parallel to that of the incident beam, respectively, as shown in Fig. 3. The value of the depolarisation ratio can further provide the information about chain conformations [51, 52] as well as the secondary structures such as molecular orientation.

3.4. Polarisability tensor and Raman tensor

In a mathematical form, the polarisability is described in general as a symmetric second-rank tensor, the so-called *polarisability tensor*. The tensor is proportional to the dipole moment of a molecule induced by the electric field of the incident beam. If the polarisability tensor of the molecule is spherically symmetric, the molecular polarisability (α) is written by the following equation, which is similar to Equation 1 but takes into account that both the electric field and the induced dipole moment are vectors,

$$\vec{\mu} = \alpha \vec{E} \quad (10)$$

where, $\vec{\mu}$ and \vec{E} represent the dipole moment of the molecule and the electric vector of the incident light in three-dimensional space, respectively. In general, however, the polarisability is not spherically symmetric; hence,

$$\vec{\mu} = [\alpha] \vec{E} \quad (11)$$

where $[\alpha]$ signifies a tensor expression of the polarisability (the *polarisability tensor*). Since a Raman tensor is given as the differential of the polarisability tensor, the Raman tensor is also considered to be a second-rank tensor, and may be given as $[\alpha']$. If the principal axes of the Raman tensor are defined as x -, y - and z -axes, the tensor

is described as,

$$[\alpha'] = \begin{pmatrix} \alpha'_{xx} & \alpha'_{xy} & \alpha'_{xz} \\ \alpha'_{yx} & \alpha'_{yy} & \alpha'_{yz} \\ \alpha'_{zx} & \alpha'_{zy} & \alpha'_{zz} \end{pmatrix} \quad (12)$$

The form of the Raman tensor is unique to the symmetry of the molecular vibration. As shown in Table I, a spherical Raman tensor has only two parameters, whereas six parameters are required to describe a general Raman tensor with no specific symmetry [38]. The forms of the Raman tensors described above refer to an individual vibration in the molecule. On the other hand, if the molecular structure has specific symmetry [31, 39], and if the molecules are packed in a crystal lattice with three-dimensional symmetry [32, 38], the Raman tensor for the vibrational mode may be written in a higher symmetrical form. In some cases [53], intra- and inter-molecular interactions might also influence the form of the tensor.

Furthermore, these symmetrical molecules and crystallites are distributed three-dimensionally in the material. Since the principal axes of the Raman tensor do not necessarily coincide with those of the molecular chain and nor of the specimen, other coordinate systems, x' - y' - z' and X - Y - Z , need to be introduced for the *molecular chain coordinate system* and *specimen coordinate system*, respectively. These coordinate systems are defined in Fig. 4, using the right-handed axes according to Bower [24]. Indeed, actual measurements for the study of molecular orientation distributions are carried out based on this specimen coordinate system. Directional information of the Raman tensor is usually obtained in terms of these specimen axes, unless a single crystal with perfect orientation is examined [54]. It is, therefore, difficult to obtain an absolute form of the Raman tensor for polymers. In general, however, the evaluation of molecular orientation does not need absolute solutions for the tensor components but only requires the ratios of the diagonal components of the tensor. Furthermore, in the case that the tensor component α'_{zz} is

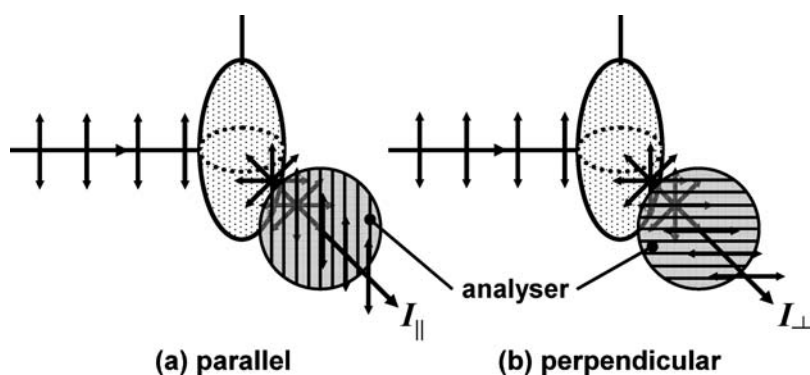
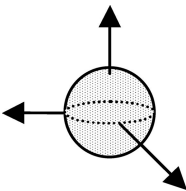
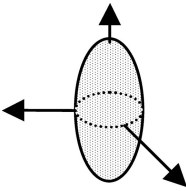
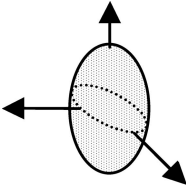


Figure 3 Scattering intensity collection of polarised Raman spectroscopy in the right angle scattering geometry. The arrows indicate the polarisation directions of incident and scattered lights. Polarisation of the scattering light through the analyser are in the directions (a) parallel and (b) perpendicular to that of the incident beam.

TABLE I Forms of Raman tensors in respect of the shape of the differential polarisability ellipsoid [38]

	Shape of the ellipsoid	Form of the Raman tensor
Spherical symmetry		$[\alpha'] = \begin{pmatrix} a & b & b \\ b & a & b \\ b & b & a \end{pmatrix}$
Cylindrical symmetry		$[\alpha'] = \begin{pmatrix} a & b & c \\ b & a & c \\ c & c & d \end{pmatrix}$
No specific symmetry		$[\alpha'] = \begin{pmatrix} a & b & c \\ b & d & e \\ c & e & f \end{pmatrix}$

much larger than the other components α'_{xx} and α'_{yy} , the Raman tensor can be approximated to have cylindrical symmetry [55].

3.5. Polarised and depolarised modes of the Raman tensor

The Raman tensor generally consists of six parameters, and it is not easy to determine all of these parameters. However, by measuring the depolarisation ratio of an isotropic sample, ρ_{iso} , additional information about the form of the Raman tensor can be obtained.

The ρ_{iso} value can be written [36, 51] as,

$$\rho_{\text{iso}} = \frac{3\bar{\gamma}'^2}{45\bar{\alpha}'^2 + 4\bar{\gamma}'^2} \quad (13)$$

where the values $\bar{\alpha}'$ and $\bar{\gamma}'^2$ are the isotropic and anisotropic part of the Raman tensor. They are given in terms of the tensor component by,

$$\bar{\alpha}' = \frac{1}{3}(\alpha'_{xx} + \alpha'_{yy} + \alpha'_{zz}) \quad (14)$$

$$\bar{\gamma}'^2 = \frac{1}{2} \{ (\alpha'_{xx} - \alpha'_{yy})^2 + (\alpha'_{yy} - \alpha'_{zz})^2 + (\alpha'_{zz} - \alpha'_{xx})^2 + 6(\alpha_{xy}^2 + \alpha_{yz}^2 + \alpha_{zx}^2) \} \quad (15)$$

in which the $\bar{\alpha}'$ value consists only of the diagonal components of the tensor, while the off-diagonal components are also included in the value $\bar{\gamma}'^2$. In other words, the former indicates the magnitude of the differential polarisability

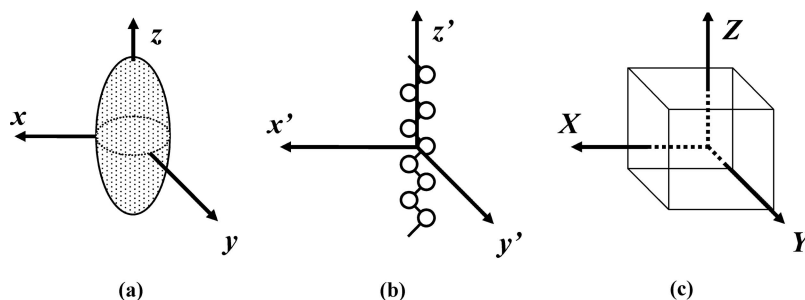


Figure 4 Definitions of the axes for (a) a Raman tensor, (b) a molecular chain and (c) a specimen.

of the molecule, and the latter represents the degree of the departure from its isotropic behaviour [26].

Referring to Equation 13, the depolarisation ratio (ρ_{iso}) for a Raman band obtained from an isotropic sample should take a value in the range between 0 and 0.75. Meanwhile, the form of a Raman tensor can be classified into two categories depending on the ρ_{iso} value. The first category gives $\rho_{\text{iso}} = 0.75$ in the case that the sum of the diagonal components of the tensor are zero, and the corresponding vibrational mode is called a *depolarised* mode. In the second category where $0 < \rho_{\text{iso}} < 0.75$, the Raman tensor contains one or more non-zero diagonal components, and it is termed a *polarised* mode. This classification is also useful for the band assignment of Raman scattering spectra.

3.6. Scattering geometry

The coordinate systems shown in Fig. 4 are correlated [38] further with each other by applying Euler angles (ϕ, θ, ψ) as represented in Fig. 5, where ϕ, θ and ψ are the azimuthal, polar and rotational angles, respectively. If the Raman tensor or the specimen shows uniaxial symmetry, the z -axis or the Z -axis is usually chosen as the symmetrical axis of the Raman tensor or of the specimen, respectively.

In Raman scattering measurements, a variety of optical geometries [26, 28, 29] can be chosen for the direction of incident beam irradiation onto a sample and that of the collection of the Raman scattering. The right angle scattering (RAS) geometry or the back scattering (BS) geometry is usually employed in consideration of the geometrical angular dependence [35] of the scattering intensity. So as to describe the optical geometry of the polarised Raman scattering, Porto's notation [56], $A(BC)D$, is often used, where A and D describe the propagation directions of the incident beam and of the direction toward the de-

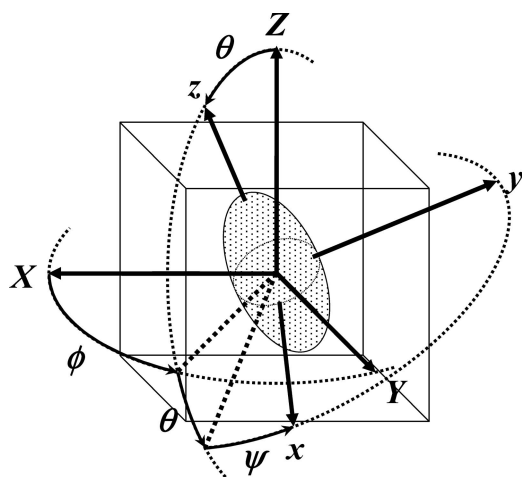


Figure 5 Definition of Euler angles (ϕ, θ, ψ) correlating the Raman tensor axes (x - y - z) and the specimen axes (X - Y - Z) [38].

tor, and B and C are the polarisation directions of the incident beam and of the analyser, respectively. For the present study, the laboratory coordinate system (X_L - Y_L - Z_L) is defined in Fig. 6. The scattering geometry shown in the figure corresponds to the notation $X_L(Z_L Y_L)X_L$, where an incident beam polarised in the Z_L -axis direction is irradiated along the X_L -axis to the sample, and the Y_L -axis component of the Raman scattering is collected through the analyser in the BS geometry. The same A - and D -axes should be chosen for the BS geometry, while a different pair of the A - and D -axes are employed for the RAS geometry.

3.7. Raman scattering intensity

The degree of interaction between the incident radiation and a molecule is dependent on the angle between the electric vector of the radiation and the shape of the polarisability tensor. The intensity of the Raman scattering changes similarly depending on the optical geometry, and the mathematical correlations between these parameters are given in this section.

As described in Section 2, an oscillating electric field of incident light induces a dipole moment in a molecule. Because of the induced dipole moment, an electric field will be induced and scattered from the molecule. Using the Maxwell equation, the scattered electric field, $\vec{E}_{sc}(t)$, at a distance r from the molecule is given [57, 58] by,

$$\vec{E}_{sc}(t) = 4\pi^2 \left(\frac{\nu_{sc}^2 \vec{\mu}(t)}{r} \right) \sin \Phi \quad (16)$$

where ν_{sc} is the frequency of the scattered radiation, Φ is the angle between the dipole axis and the scattering direction. The term $\vec{\mu}(t)$ is the induced dipole moment as defined in Equation 10, and is time dependent since the electric field vector, $\vec{E}_{in}(t)$, of the incident light changes with time. They are related as in Equation 10 by,

$$\vec{\mu}(t) = \alpha \vec{E}_{in}(t) \quad (10')$$

The scattering intensity from the induced dipole moment, I_{sc} , is given by the following equation [26],

$$I_{sc} = |\vec{E}_{sc}|^2 r^2 = 2^4 \pi^4 |\alpha|^2 \nu_{sc}^4 |\vec{E}_{in}|^2 \sin^2 \Phi \quad (17)$$

Here, it is worth noticing that the scattering will be observed except in the direction of the dipole axis, i.e. $\Phi = 0^\circ$.

By recalling the molecular polarisability (α) in Equation 4 and the dipole moment in Equation 5, the Rayleigh scattering component of I_{sc} should be proportional to the

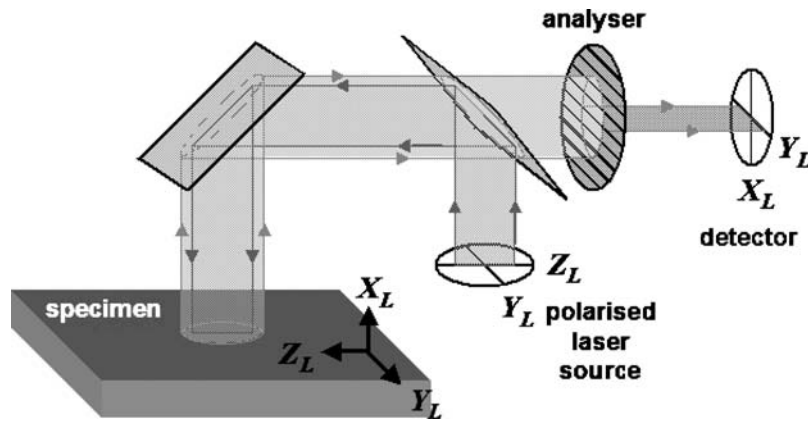


Figure 6 An example of the collection of the polarised Raman scattering for the back scattering geometry $X_L(Z_L Y_L)X_L$.

value of $|\alpha|^2$. On the other hand, the Stokes and anti-Stokes Raman scattering intensities should be proportional to the value of $|\frac{\partial \alpha}{\partial q_k}|^2$, in other words $|\alpha'|^2$.

Using the Raman tensor (α'), the I_{sc} for Stokes Raman scattering ($I_{sc-Stokes}$) over a solid angle of 4π can be written by [29],

$$I_{sc-Stokes} = \frac{2^7 \pi^5}{3^2 c^4} I_{in} (v_o - v_m)^4 \sum_{ij} |\alpha'_{ij}|^2 \quad (18)$$

where c is the speed of light, I_{in} is the intensity of the incident light, α'_{ij} is the (i, j) -th component of the Raman tensor, and i, j are directions of the scattered and incident light, respectively. Based on the theory of electromagnetic waves [28],

$$I_{in} = \frac{c}{8\pi} |\vec{E}_{in}|^2 \quad (19)$$

Therefore, Equation 18 becomes,

$$I_{sc-Stokes} = \frac{2^4 \pi^4}{3^2 c^3} |\vec{E}_{in}|^2 (v_o - v_m)^4 \sum_{ij} |\alpha'_{ij}|^2 \quad (20)$$

3.8. Intensity of polarised Raman scattering

The Stokes Raman scattering intensity ($I_{sc-Stokes}$) in Equation 20 is the summation over a solid angle of 4π . When an analyser is used to detect the Raman scattering with a specific electric vector only, the Raman intensity can further provide information on the Raman tensor of the molecule and its distribution within the specimen. A theory to explain this phenomenon was introduced by Bower [24] in combination with the previous studies on the Raman scattering intensity [32, 38] and molecular orientation in the material [9, 34]. Most of the studies on polarised Raman spectroscopy have based their theoretical expressions for the polarised

Raman intensity on a study [24] by Bower and a review [8] by Ward.

Equation 20 can be simplified for a Raman scattering intensity per solid angle, I_s , and given by the following equation in consideration of the polarisation directions of the incident and scattered light,

$$I_s = I_o \left| \vec{l}_g' \alpha' \vec{l}_g \right|^2 \quad (21)$$

where I_o summarises constants in Equation 20 if information about the incident light and molecular vibration is provided. The terms g and g' signify the polarised direction of the incident beam and that of an analyser, respectively, \vec{l}_g and $\vec{l}_{g'}$ are the direction cosines of the incident and of the scattered beam along the g and g' directions, respectively.

The intensity I_s in Equation 21 is for a single molecule, and for the molecules over the whole irradiation volume in the sample are given as their summation by,

$$I_S = I_o \sum \left| \vec{l}_g' \alpha' \vec{l}_g \right|^2 \quad (22)$$

In respect of the term I_s in Equation 17, Bower [24] also introduced an alternative form, given by the following equation to correlate scattered intensities collected from different optical geometries:

$$I_S = I_o \sum \alpha'_{g'g} \alpha'_{p'p} \quad (23)$$

where the subscript ($g' g p' p$) is restricted to a form of either $(i i j j)$ or $(i j i j)$ owing to the symmetry of Raman tensors. For instance, if the analyser measures the intensity of the Y -axis component of the Raman scattering from the sample irradiated by an incident beam polarised in the Z -axis, the term I_s is expressed by,

$$I_S = I_o \sum \alpha'_{YZ} \alpha'_{YZ} = I_o \sum \alpha'^2_{YZ} \quad (23')$$

When Equation 22 is considered for a single crystal with perfect molecular orientation [32], where the x - y - z Raman tensor axes are identical to the X - Y - Z specimen axes, the scattering intensity I_S can be written using a matrix [54] for the optical geometry used in Equation 23' as,

$$I_S = I_o \sum \left[\sum_{YZ} (0 \ 1 \ 0) \begin{pmatrix} \alpha'_{xx} & \alpha'_{xy} & \alpha'_{xz} \\ \alpha'_{yx} & \alpha'_{yy} & \alpha'_{yz} \\ \alpha'_{zx} & \alpha'_{zy} & \alpha'_{zz} \end{pmatrix} \begin{pmatrix} 0 \\ 0 \\ 1 \end{pmatrix} \right]^2 = I_o \sum \alpha'^2_{yz} \quad (22')$$

In fact, the axes (x - y - z) for the Raman tensor are usually not coincident with the axes (X - Y - Z) for the sample for polycrystalline materials, or semicrystalline and amorphous materials. Furthermore, the principal axes of Raman tensor may not be consistent with the molecular axes (x' - y' - z') defined in Fig. 4b. For these systems the Raman scattering intensity can be correlated with the Raman tensor by the orientation distribution functions, provided that the tensor is independent of sample morphology. Some studies reported that the Raman tensors of some bands could be influenced by factors such as the semicrystalline nature of the sample [59] or by deformation [60]. However, most of the studies have been performed successfully by assuming an invariant Raman tensor.

3.9. Orientation distribution function: $N(\phi, \theta, \psi)$

3.9.1. Expansion coefficients: v_{lmn}

According to Bower [24], the *orientation distribution function*, $N(\phi, \theta, \psi)$, is introduced to describe molecular orientation distributions, where $N(\phi, \theta, \psi) \sin\theta d\theta d\psi d\phi$ represents the fraction of scattering units having orientation within a generalised solid angle $\sin\theta d\theta d\psi d\phi$ by using Euler angles in Fig. 5. The function $N(\phi, \theta, \psi)$ can be written [34, 61, 62] by the following equation as a function of $\cos \theta$:

$$N(\phi, \xi, \psi) = \sum_{l=0}^{\infty} \sum_{m=-l}^l \sum_{n=-l}^l v_{lmn} Z_{lmn}(\xi) e^{-im\psi} e^{-in\phi} = \sum_{lmn} v_{lmn} Z_{lmn}(\xi) e^{-im\psi} e^{-in\phi} \quad (24)$$

where $\xi = \cos\theta$, the terms v_{lmn} and $Z_{lmn}(\xi)$ are the expansion coefficients and the generalised Legendre polynomials of the lmn orders, respectively. The expansion coefficients (v_{lmn}) can be derived from Equation 24 as,

$$v_{lmn} = \frac{1}{4\pi^2} \int_0^{2\pi} \int_0^{2\pi} \int_{-1}^1 N(\phi, \xi, \psi) Z_{lmn}$$

$$\times (\xi) e^{im\psi} e^{in\phi} d\xi d\psi d\phi \quad (25)$$

On the other hand, the polarised Raman intensity can be described in a similar way by,

$$\sum \alpha'_{g'g} \alpha'_{p'p} = N_o \int_0^{2\pi} \int_0^{2\pi} \int_{-1}^1 N(\phi, \xi, \psi) \alpha'_{g'g} \alpha'_{p'p} d\xi d\psi d\phi \quad (26)$$

where the term $\alpha'_{g'g} \alpha'_{p'p}$ is a tensor expression of the interaction between polarised light and the differential polarisability of a scattering unit, and N_o is the number of scattering units in the sample. The term inside the integral in Equation 26 can be replaced by the expansion coefficients (v_{lmn}) and coefficients ($A_{lmn}^{g'g p'p}$) related to Raman tensor components as,

$$\sum \alpha'_{g'g} \alpha'_{p'p} = N_o \sum_{lmn} v_{lmn} A_{lmn}^{g'g p'p} \quad (27)$$

As mentioned in the previous section, the Raman tensor axes (x - y - z) are not necessarily coincident with the molecular axes (x' - y' - z'). Therefore, the expansion coefficients (v_{lmn}) can be explained in terms of these axes by introducing two sets of expansion coefficients (M_{lmn} , D_{lmn}) as,

$$\sum \alpha'_{g'g} \alpha'_{p'p} = 16\pi^4 N_o \sum_{lmn\zeta} \sqrt{\frac{2}{2l+1}} M_{lm\zeta} D_{l\zeta n} A_{lmn}^{g'g p'p} \quad (28)$$

where $M_{lm\zeta}$ and $D_{l\zeta n}$ represent expansion coefficients of the molecular axes (x' - y' - z') to the specimen axes (X - Y - Z), and of the Raman tensor axes (x - y - z) to the molecular chain axes (x' - y' - z'), respectively. These three expansion coefficients (v_{lmn} , $M_{lm\zeta}$, $D_{l\zeta n}$) are correlated by,

$$v_{lmn} = 4\pi^2 \sqrt{\frac{2}{2l+1}} \sum_{\zeta=-l}^l M_{lm\zeta} D_{l\zeta n} \quad (29)$$

In practice, however, most of the previous studies assume that the Raman tensor axes (x - y - z) are coincident with the molecular axes (x' - y' - z') to reduce the number of parameters for the determination of the distribution coefficients (v_{lmn}). Under this assumption,

$$D_{l\zeta n} = \frac{1}{8\pi^2} \sqrt{\frac{2l+1}{2}} \quad (30)$$

TABLE II Values of $A_{lmn}^{g'gp'p}$ for a Raman tensor with cylindrical symmetry in a specimen with uniaxial or biaxial symmetry [24]

$\alpha'_{g'g}\alpha'_{p'p}$	A ₀₀₀	A ₂₀₀	A ₄₀₀	A ₂₂₀	A ₄₂₀	A ₄₄₀
α'^2_{XX}	A	4B	6C	$-2\sqrt{6}B$	$-2\sqrt{10}C$	$\sqrt{70}C$
α'^2_{YY}	A	4B	6C	$2\sqrt{6}B$	$2\sqrt{10}C$	$\sqrt{70}C$
α'^2_{ZZ}	A	-8B	16C	0	0	0
α'^2_{XY}	D	4E	2C	0	0	$-\sqrt{70}C$
α'^2_{YZ}	D	-2E	-8C	$\sqrt{6}E$	$-2\sqrt{10}C$	0
α'^2_{ZX}	D	-2E	-8C	$-\sqrt{6}E$	$2\sqrt{10}C$	0
$\alpha'_{XX}\alpha'_{YY}$	A-2D	4B-8E	2C	0	0	$-\sqrt{70}C$
$\alpha'_{YY}\alpha'_{ZZ}$	A-2D	-2B+4E	-8C	$\sqrt{6}(B-2E)$	$-2\sqrt{10}C$	0
$\alpha'_{ZZ}\alpha'_{XX}$	A-2D	-2B+4E	-8C	$\sqrt{6}(2E-B)$	$2\sqrt{10}C$	0

$$A = \frac{\sqrt{2}}{15} \left[3(\alpha'^2_{xx} + \alpha'^2_{yy} + \alpha'^2_{zz}) + 2(\alpha'_{xx}\alpha'_{yy} + \alpha'_{yy}\alpha'_{zz} + \alpha'_{zz}\alpha'_{xx}) \right].$$

$$B = \frac{1}{210} \sqrt{\frac{5}{2}} \left[3\alpha'^2_{xx} + 3\alpha'^2_{yy} - 6\alpha'^2_{zz} + 2\alpha'_{xx}\alpha'_{yy} - \alpha'_{yy}\alpha'_{zz} - \alpha'_{zz}\alpha'_{xx} \right].$$

$$C = \frac{1}{840\sqrt{2}} \left[3\alpha'^2_{xx} + 3\alpha'^2_{yy} + 8\alpha'^2_{zz} + 2\alpha'_{xx}\alpha'_{yy} - \alpha'_{yy}\alpha'_{zz} - \alpha'_{zz}\alpha'_{xx} \right].$$

$$D = \frac{\sqrt{2}}{15} \left[\alpha'^2_{xx} + \alpha'^2_{yy} + \alpha'^2_{zz} - (\alpha'_{xx}\alpha'_{yy} + \alpha'_{yy}\alpha'_{zz} + \alpha'_{zz}\alpha'_{xx}) \right].$$

$$E = \frac{1}{210} \sqrt{\frac{5}{2}} \left[\alpha'^2_{xx} + \alpha'^2_{yy} - 2\alpha'^2_{zz} - 4\alpha'_{xx}\alpha'_{yy} + 2\alpha'_{yy}\alpha'_{zz} + 2\alpha'_{zz}\alpha'_{xx} \right].$$

for $\zeta = \pm n$, and the values $D_{l\zeta n}$ will be zero otherwise. Equation 28 can be simplified as,

$$\sum \alpha'_{g'g}\alpha'_{p'p} = 4\pi^2 N_o \sum_{lmn} M_{lmn} A_{lmn}^{g'gp'p} \quad (31)$$

which is similar to Equation 27.

Here, the left-hand side of Equation 27 can be evaluated experimentally by the measurement of I_S (Equation 23), while the values $A_{lmn}^{g'gp'p}$ in the right-hand side can be calculated from the Raman tensor components for the orders of lmn according to Bower [24]. Although the value of $A_{lmn}^{g'gp'p}$ should be derived for each M_{lmn} value according to Equations 27 and 29, they can be simplified [24] if the Raman tensor has specific symmetry. The $A_{lmn}^{g'gp'p}$ values corresponding to the non-vanished M_{lmn} terms are listed in Table II with respect to the intensity $\sum \alpha'_{g'g}\alpha'_{p'p}$ for a Raman tensor with cylindrical symmetry in a specimen with uniaxial or biaxial symmetry. Therefore, it is possible to determine the expansion coefficients (v_{lmn}) for the Raman tensor with respect to the specimen axes.

Furthermore, the symmetry of the specimen can also reduce the number of equations required to determine the values v_{lmn} [55, 63]. By combining the polarisation direction of the incident beam and that of the analyser, six independent Raman scattering intensities are measurable for a sample with biaxial symmetry, whereas the four intensities are independent for one with uniaxial symmetry. In an extreme case, only two different intensities can be obtained for a sample with spherical symmetry as summarised in Table III.

TABLE III Number of independent Raman scattering intensities with respect to the specimen symmetry [55, 63]

Specimen symmetry	Number of independent intensities	
Spherical (isotropic)	2	$XX=YY=ZZ^*$ $XY=YZ=ZX=XZ=ZY=YX$
Uniaxial	4	$XX=YY$ $XY=YX$ ZZ $YZ=ZX=XZ=ZY$
Biaxial	6	XX $XY=YX$ YY $YZ=ZY$ ZZ $ZX=XZ$
General (no symmetry)	9	All independent

(*) Polarisation direction of incident and scattered beams

4. Molecular orientation distribution coefficients: P_{lmn}

In the previous section, it was shown that information about the molecular orientation distributions in the sample can be provided in terms of the expansion coefficients (v_{lmn}). Although Equation 27 shows simple correlations between Raman tensor components and the polarised Raman scattering intensities for different polarisation geometries, these equations contain a number of the coefficients (v_{lmn}) that need to be determined. However, the process of obtaining the coefficients v_{lmn} can be simplified [39] (a) by assuming that the Raman tensor axes (x - y - z) are coincident with the molecular axes (x' - y' - z'), (b) if the Raman tensor possesses certain symmetry, and (c) if the specimen has axial orientation symmetry.

It is also of importance that the molecular orientation distributions determined by polarised Raman spectroscopy can be compared with those obtained from other techniques such as X-ray diffraction and birefringence measurements. In these techniques, the

molecular orientation distributions are often described in terms of the *molecular orientation distribution coefficients*, P_{lmn} , and *molecular orientation distribution parameters*, $\langle \cos^l \theta \rangle$, the details of which are explained in the following section. Hereafter, relationships between these coefficients and parameters are considered for two types of symmetries in the sample, in particular, uniaxial and biaxial orientations.

4.1. The P_{lmn} values for a sample with uniaxial orientation

According to references [8, 40, 48, 64], the simplest system that can be considered is a Raman tensor with cylindrical symmetry and a specimen with uniaxial symmetry around the draw axis. For a sample with uniaxial symmetry, the P_{lmn} values are non-zero only when $m = n = 0$ and $l = \text{even}$ (0, 2, 4, ...), and they are correlated with the function $N(\theta)$ in Equation 24 by,

$$P_{l00} = \frac{\int_0^\pi N(\theta) P_{l00}(\cos \theta) \sin \theta d\theta}{\int_0^\pi N(\theta) \sin \theta d\theta} \quad (32)$$

where the fraction of polymer chains at an angle θ is given as $N(\theta)d\theta$. The functions $P_{l00}(\cos \theta)$ are Legendre polynomial functions of $\cos \theta$, $P_{l00}(\cos \theta) = 1/2$, and the functions for the orders of $l = 2, 4$ are:

$$P_{200}(\cos \theta) = \frac{3 \cos^2 \theta - 1}{2} \quad (33)$$

$$P_{400}(\cos \theta) = \frac{35 \cos^4 \theta - 30 \cos^2 \theta + 3}{8} \quad (34)$$

As depicted in Fig. 7, the function $N(\theta)$ can be normalised [8, 40] by,

$$2\pi \int_0^\pi N(\theta) \sin \theta d\theta = 1 \quad (35)$$

After the normalisation, the molecular orientation distribution function $N(\theta)$ is related [3, 8, 40, 48, 49] further to the molecular orientation distribution coefficients (P_{lmn}) by,

$$N(\theta) = \sum_{l=0}^{\infty} \left(\frac{2l+1}{2} \right) P_{l00} P_{l00}(\cos \theta) \quad (36)$$

for a uniaxially-oriented specimen.

Under the assumption where the axes (x - y - z) of the Raman tensor coincide with those (x' - y' - z') of the molecular chain, the molecular orientation distribution coefficients (P_{l00}) are correlated with the expansion coefficients (M_{l00})

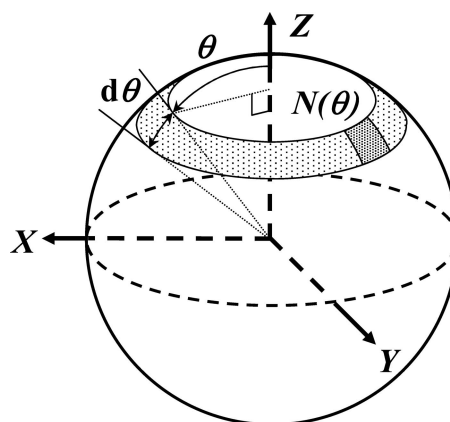


Figure 7 Schematic representation for the determination of the molecular orientation distribution coefficients.

determined from polarised Raman spectroscopy by,

$$P_{l00} = 4\pi^2 \sqrt{\frac{2}{2l+1}} M_{l00} \quad (37)$$

which is a simplified form [65, 66] of Equation 29.

On the other hand, the molecular orientation distribution parameters [3, 48, 67], $\langle \cos^l \theta \rangle$, are also regarded as meaningful measures of molecular orientation distributions. The angle θ represents the angle between the principal z -axis of the Raman tensor and of the specimen Z -axis, as defined in Fig. 7. The brackets ' $\langle \rangle$ ' average the angular distribution of the molecular chains with respect to the angle θ over the sample. These values are determined by the following equation:

$$\langle \cos^l \theta \rangle = \frac{\int_0^\pi N(\theta) \cos^l \theta \sin \theta d\theta}{\int_0^\pi N(\theta) \sin \theta d\theta} \quad (38)$$

which is similar to Equation 32. Relationships between the coefficients P_{l00} and the parameters $\langle \cos^l \theta \rangle$ are given further by,

$$P_{000} = 1 \quad (39)$$

$$P_{200} = \frac{1}{2} [3 \langle \cos^2 \theta \rangle - 1] \quad (40)$$

$$P_{400} = \frac{1}{8} [35 \langle \cos^4 \theta \rangle - 30 \langle \cos^2 \theta \rangle + 3] \quad (41)$$

for the orders of $l = 0, 2, 4$. It can be seen in Equation 40 that the coefficient P_{200} is identical to the Hermans' orientation coefficient [68].

4.2. The P_{lmn} values for a sample with uniaxial orientation

The forms of the molecular orientation distribution coefficients (P_{lmn}) are more complicated for a specimen with biaxial orientation. For simplicity, it is assumed that the axes (x - y - z) of the Raman tensor coordinate system are consistent with those (x' - y' - z') of the molecular coordinate system. Relationships between the P_{lmn} values and the parameters ($\cos^l \theta$) can be classified [7] into four cases depending on the symmetry of molecular orientation distribution, provided that the Raman tensor has cylindrical symmetry.

(i) *Uniaxial orientation about the Z-axis and no preferred orientation about the z-axis*: the structural units are randomly distributed around the z -axis, and the z -axis is also randomly distributed around the specimen Z -axis. In other words, there is no restriction of the angle ψ and ϕ , which is the same case as the expression for a sample with uniaxial orientation given in the previous section.

(ii) *Biaxial orientation but with no preferred orientation about the z-axis*: the angle ψ is random but not the angle ϕ in this case. The P_{lmn} values are non-zero only for $n = 0$, and are written by,

$$P_{220} = \frac{1}{4} \langle (1 - \cos^2 \theta) \cos 2\phi \rangle \quad (42)$$

$$P_{420} = \frac{1}{24} \langle (-1 + 8 \cos^2 \theta - 7 \cos^4 \theta) \cos 2\phi \rangle \quad (43)$$

$$P_{440} = \frac{1}{16} \langle (1 - 2 \cos^2 \theta + \cos^4 \theta) \cos 4\phi \rangle \quad (44)$$

in addition to the P_{l00} values determined for case (i).

(iii) *General uniaxial statistical symmetry*: the angle ϕ is random but not ψ in this case. The non-zero values for P_{lmn} are only for $m = 0$, and the corresponding expressions are:

$$P_{202} = \frac{1}{4} \langle (1 - \cos^2 \theta) \cos 2\psi \rangle \quad (45)$$

$$P_{402} = \frac{1}{24} \langle (-1 + 8 \cos^2 \theta - 7 \cos^4 \theta) \cos 2\psi \rangle \quad (46)$$

$$P_{404} = \frac{1}{16} \langle (1 - 2 \cos^2 \theta + \cos^4 \theta) \cos 4\psi \rangle \quad (47)$$

in addition to the P_{lmn} values determined for cases (i) and (ii).

(iv) *General biaxial statistical symmetry*: in the most constrained biaxial symmetry neither the angle ψ nor ϕ is random, which results in the whole P_{lmn} values to be non-zero and are written by,

$$P_{222} = \frac{1}{4} \langle (1 + \cos^2 \theta) \cos 2\phi \cos 2\psi - 2 \cos \theta \sin 2\phi \sin 2\psi \rangle \quad (48)$$

$$P_{422} = \frac{1}{4} \langle (1 - 6 \cos^2 \theta + 7 \cos^4 \theta) \cos 2\phi \cos 2\psi + (5 \cos \theta - 7 \cos^3 \theta) \sin 2\phi \sin 2\psi \rangle \quad (49)$$

$$P_{442} = \frac{1}{16} \langle (1 - \cos^4 \theta) \cos 4\phi \cos 2\psi - 2(\cos \theta - \cos^3 \theta) \sin 4\phi \sin 2\psi \rangle \quad (50)$$

$$P_{424} = \frac{1}{16} \langle (1 - \cos^4 \theta) \cos 2\phi \cos 4\psi - 2(\cos \theta - \cos^3 \theta) \sin 2\phi \sin 4\psi \rangle \quad (51)$$

$$P_{444} = \frac{1}{16} \langle (1 + 6 \cos^2 \theta + \cos^4 \theta) \cos 4\phi \cos 4\psi - 4(\cos \theta + \cos^3 \theta) \sin 4\phi \sin 4\psi \rangle \quad (52)$$

in addition to the P_{lmn} values determined for cases (i), (ii) and (iii).

These molecular orientation distribution coefficients P_{lmn} are related [34] to the expansion coefficients ν_{lmn} obtained from polarised Raman spectroscopy by,

$$P_{lmn} = \frac{4\pi^2}{N_{lmn}} \nu_{lmn} \quad (53)$$

where,

$$N_{lmn}^2 = N_{l\bar{m}n}^2 = N_{l\bar{m}\bar{n}}^2 = N_{l\bar{m}\bar{n}}^2 = \frac{2l+1}{2} \times \frac{(l+m)!(l-n)!}{(l-m)!(l+n)!} \frac{1}{[(m-n)!]^2} \quad (54)$$

for $m > n$, and,

$$N_{lmn}^2 = N_{l\bar{m}n}^2 \quad (55)$$

for $m < n$. Equation 54 is regarded as generalised expressions of Equation 37.

On the other hand, an average of the angular distribution between the axes (x - y - z) of the Raman tensor coordinate system and those (X - Y - Z) of the specimen coordinate system can be given [7] by the following equations in terms of the molecular orientation distribution coefficients of the second order (P_{2mn}),

$$\langle \cos^2(\angle xX) \rangle = \frac{1}{3} + \frac{1}{6} P_{200} - P_{220} - P_{202} + P_{222} \quad (56)$$

$$\langle \cos^2(\angle xY) \rangle = \frac{1}{3} + \frac{1}{6} P_{200} + P_{220} - P_{202} - P_{222} \quad (57)$$

$$\langle \cos^2(\angle xZ) \rangle = \frac{1}{3} - \frac{1}{3} P_{200} + 2P_{202} \quad (58)$$

$$\langle \cos^2(\angle yX) \rangle = \frac{1}{3} + \frac{1}{6}P_{200} - P_{220} + P_{202} - P_{222} \quad (59)$$

$$\langle \cos^2(\angle yY) \rangle = \frac{1}{3} + \frac{1}{6}P_{200} + P_{220} + P_{202} + P_{222} \quad (60)$$

$$\langle \cos^2(\angle yZ) \rangle = \frac{1}{3} - \frac{1}{3}P_{200} - 2P_{202} \quad (61)$$

$$\langle \cos^2(\angle zX) \rangle = \frac{1}{3} - \frac{1}{3}P_{200} + 2P_{220} \quad (62)$$

$$\langle \cos^2(\angle zY) \rangle = \frac{1}{3} - \frac{1}{3}P_{200} - 2P_{220} \quad (63)$$

$$\langle \cos^2(\angle zZ) \rangle = \frac{1}{3} + \frac{2}{3}P_{200} \quad (64)$$

where $\langle \cos^2(\angle iJ) \rangle$ is an average of the angular distribution of the i -axis of the Raman tensor with respect to the J -axis of the specimen.

4.3. The (P_{200}, P_{400}) window

For a sample with a uniaxial orientation distribution, the molecular orientation distribution coefficients P_{l00} need to be determined [3] for all the orders of l so as to obtain the molecular orientation distribution function $N(\theta)$ in Equation 36. In fact, different molecular distributions can give an identical P_{200} value [61]. It is, however, possible to predict [40, 41] the types of distributions from the P_{200} and P_{400} values.

First of all, relationships between the $\langle \cos^2 \theta \rangle$ and $\langle \cos^4 \theta \rangle$ values give boundaries of the P_{200} and P_{400} values to be taken. According to the Schwarz inequality [2, 40, 41],

$$\langle \cos^2 \theta \rangle^2 \leq \langle \cos^4 \theta \rangle \quad (65)$$

and clearly,

$$\langle \cos^4 \theta \rangle \leq \langle \cos^2 \theta \rangle \quad (66)$$

Using Equations 40 and 41, the P_{400} value is limited by a function of P_{200} by,

$$\frac{35P_{200}^2 - 10P_{200} - 7}{18} \leq P_{400} \leq \frac{5P_{200} + 7}{12} \quad (67)$$

These boundaries are shown as a linear line (A-B) and a curve (A-C-B) in Fig. 8a, where the points O(0, 0), A(1, 1) and B(-1/2, 3/8) correspond to the (P_{200}, P_{400}) values for a sample with random molecular orientation (O in Fig. 8b), with perfect orientation along the specimen Z-

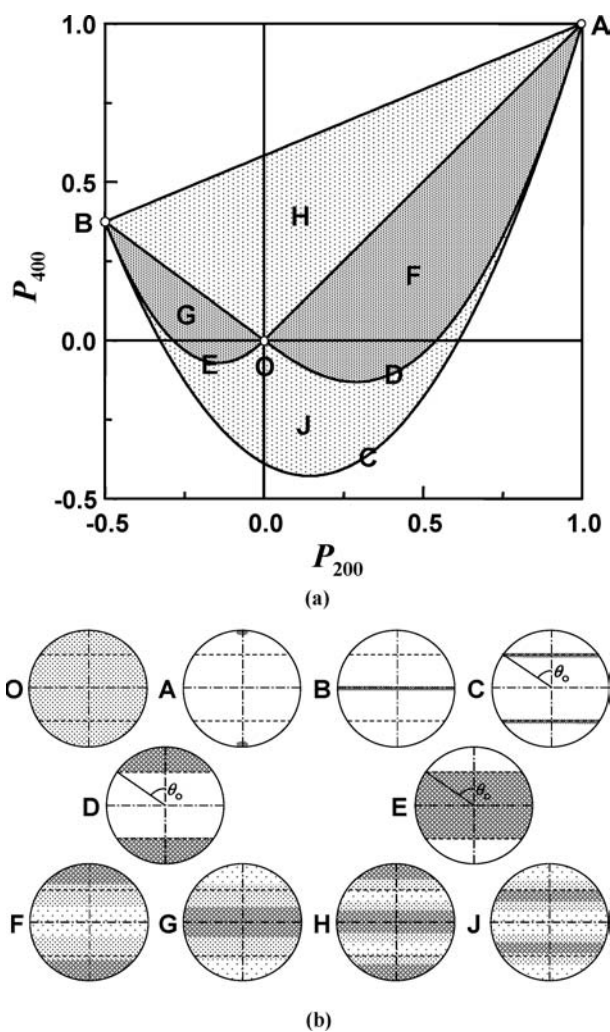


Figure 8 (a) Limitations of P_{200} and P_{400} values [40, 41], and (b) corresponding molecular orientation distributions in a uniaxially-oriented sample (the darker the shadow, the higher the molecular orientation; the vertical line is in the direction parallel to the specimen Z-axis).

axis (A), and with perfect orientation normal to the Z-axis (B), respectively.

Next, real distributions can be assumed using two-phase models, where one phase has perfect orientation and the other phase has random orientation. The (P_{200}, P_{400}) values depend on the ratio of these two phases, which are shown as two lines, (A-O) and (B-O), in Fig. 8a.

The other boundaries can be given by considering the models in which functions $N(\theta)$ are assumed to be single-step functions. Two cases are taken into account: (i) the function $N(\theta)$ is constant at $0^\circ \leq \theta \leq \theta_0$ and zero at $\theta_0 \leq \theta \leq 90^\circ$ (D in Fig. 8b), (ii) the function $N(\theta)$ is zero at $0^\circ \leq \theta \leq \theta_0$ and constant at $\theta_0 \leq \theta \leq 90^\circ$ (E). The integral in Equation 32 gives,

$$P_{200} = \frac{\cos \theta_0 (1 + \cos \theta_0)}{2} \quad (68)$$

$$P_{400} = \frac{\cos \theta_0 (1 + \cos \theta_0) (7 \cos^2 \theta_0 - 3)}{8} \quad (69)$$

for case (i) and,

$$P_{200} = \frac{\cos \theta_0 (\cos^2 \theta_0 - 1)}{2} \quad (70)$$

$$P_{400} = \frac{\cos \theta_0 (\cos^2 \theta_0 - 1) (7 \cos^2 \theta_0 - 3)}{8} \quad (71)$$

for case (ii). The (P_{200}, P_{400}) correlations for cases (i) and (ii) are shown in Fig. 8a as the curves (O-D-B) and (O-E-A), respectively.

Finally, molecular orientation distributions are divided by these boundaries in Fig. 8a into four types: (i) a monotonic decrease of the function $N(\theta)$ with increasing θ (F in Fig. 8b), (ii) a monotonic increase of the function $N(\theta)$ with increasing θ (G), (iii) the function $N(\theta)$ has at least one minimum at θ_0 where $0^\circ < \theta_0 < 90^\circ$ (H), and (iv) the function $N(\theta)$ has at least one maximum at θ_0 where $0^\circ < \theta_0 < 90^\circ$ (J).

The diagram in Fig. 8a is useful [2] to obtain information about the molecular orientation distribution when the values of P_{200} and P_{400} are derived experimentally.

5. Most probable orientation distribution function: $N_{mp}(\phi, \theta, \psi)$

The P_{lmn} values with the order l higher than 4 influence the function $N(\phi, \theta, \psi)$ when a sample has high molecular orientation. It is, however, not easy to obtain these higher-order P_{lmn} values apart from by using X-ray diffraction. On the other hand, the function $N(\phi, \theta, \psi)$ for such a sample may be predicted [22, 23, 45, 46] as the *most probable molecular orientation distribution function*, $N_{mp}(\phi, \theta, \psi)$, using information entropy theory [40, 42–44]. According to the theory, unknown parameters of the system can be postulated to maximise the entropy of the system.

By following the mathematical derivation given in the Appendix, the information entropy of the distribution function $S[N(\phi, \theta, \psi)]$ is given [42–44] by,

$$S[N(\phi, \theta, \psi)] = - \int_0^\pi \int_0^{2\pi} \int_0^{2\pi} N(\phi, \theta, \psi) \ln N(\phi, \theta, \psi) d\psi d\phi d\theta \quad (73)$$

under the following constraints,

$$N(\phi, \theta, \psi) \geq 0 \quad (74)$$

and

$$\int_0^\pi \int_0^{2\pi} \int_0^{2\pi} N(\phi, \theta, \psi) \sin \theta d\psi d\phi d\theta = 1 \quad (75)$$

By introducing the Lagrange multipliers A_{lmn}^{mp} for the known P_{lmn} values ($l = 2$ and 4 in the case of polarised Raman spectroscopy) and by maximising the entropy $S[N(\phi, \theta, \psi)]$, Equation 73 becomes,

$$\int_0^\pi \int_0^{2\pi} \int_0^{2\pi} \left[\ln N(\phi, \theta, \psi) - \sum_{lmn} A_{lmn}^{mp} P_{lmn}(\phi, \cos \theta, \psi) \right] \delta N(\phi, \theta, \psi) \times \sin \theta d\psi d\phi d\theta = 0 \quad (76)$$

which gives,

$$N_{mp}(\theta, \phi, \psi) = \frac{\exp \left[\sum_{lmn} A_{lmn}^{mp} P_{lmn}(\phi, \cos \theta, \psi) \right]}{\int_0^\pi \int_0^{2\pi} \int_0^{2\pi} \exp \left[\sum_{lmn} A_{lmn}^{mp} P_{lmn}(\phi, \cos \theta, \psi) \right] \sin \theta d\psi d\phi d\theta} \quad (77)$$

where the functions $P_{lmn}(\phi, \cos \theta, \psi)$ take the forms of equations from (39) to (52) without brackets ' $\langle \rangle$ ', and the terms A_{lmn}^{mp} are constrained to satisfy the P_{lmn} values in the following equations,

$$P_{lmn} = \frac{\int_0^\pi \int_0^{2\pi} \int_0^{2\pi} N_{mp}(\phi, \theta, \psi) P_{lmn}(\phi, \cos \theta, \psi) \sin \theta d\psi d\phi d\theta}{\int_0^\pi \int_0^{2\pi} \int_0^{2\pi} N_{mp}(\phi, \theta, \psi) \sin \theta d\psi d\phi d\theta} \quad (78)$$

which are corresponding to the Equation 32 generalised for all the P_{lmn} values.

The information entropy theory described above is also applicable for other techniques such as IR dichroism measurements where P_{lmn} values of $l = 2$ only can be obtained. However, the function $N_{mp}(\phi, \theta, \psi)$ predicted by polarised Raman spectroscopy would expect to be closer to the true distribution function $N(\phi, \theta, \psi)$ than that by IR dichroism measurements with respect to the number of the constraints considered in Equation 78.

6. Factors affecting the evaluation of the Raman scattering intensity

In principle, a set of polarised Raman spectra can be interpreted in terms of molecular orientation distribution coefficients through the theoretical treatment above. However, the spectra might have already been distorted by

several factors such as intrinsic characteristics of the material, sample geometry and instrumental factors. Therefore, special care should be taken for the determination of the polarised Raman scattering intensity as described in the following sections.

6.1. Intrinsic characteristics of the material

6.1.1. The tilt angle, Ω

As described in Section 3.8, the P_{lmn} values measured using polarised Raman spectroscopy contain information about the orientation distribution of the Raman tensors for the Raman band. However, the principal axis of the Raman tensor is not necessarily coincident with that of the molecular chain. In order to obtain information about the orientation distribution of molecular chains, the P_{lmn} values for the Raman tensor need to be corrected using the angular relationships between the x - y - z Raman tensor coordinate and the x' - y' - z' molecular chain coordinate, which are shown by Equation 29. In general, however, three more parameters using Euler angles are required to correlate these two coordinates.

However, the correction process can be simplified if the Raman tensor has cylindrical symmetry. The P_{lmn} values of the molecular chain ($P_{lmn,chain}$) are related to those of the Raman tensor (P_{lmn}) [69–71] using the following equation by introducing a *tilt angle*, Ω ,

$$P_{lmn,chain} = \frac{1}{P_{lmn}(\cos \Omega)} P_{lmn} \quad (79)$$

where the angle Ω is defined as the angle between the principal axis of a Raman tensor and the molecular chain axis.

6.1.2. Overlapping of vibrational modes

Since polymers in general consist of a limited variety of elements (H, C, O, N) and since their masses are relatively similar (apart from the hydrogen atom), molecules contain a number of vibrational modes with similar energy levels. In semicrystalline polymers, the positions of the Raman bands assigned to their amorphous phases may also differ slightly [72] from the ones assigned to the crystalline phases. As a result, the Raman spectra assigned to these bands are often overlapped, which affects the quantification of the Raman intensity. A curve fitting procedure is a useful approach to deconvolute these overlapped peaks. However, fitting parameters should be chosen carefully since the mathematical best fitting does not necessarily represent the actual peaks due to an insufficient S/N ratio or a shift due to polarisation.

If a pair of the vibrational modes assigned to the *A* and *E* classes are overlapped, only the *A*-class band would be obtained for isotropic samples. This can be done [30,

36] simply by subtracting the 4/3 times of the intensity of the spectra in the $X_L(Z_L Y_L)X_L$ geometry from the intensity of the spectra in the $X_L(Z_L Z_L)X_L$ geometry according to Equations 9 and 13. This technique could be useful to separate the strongly-polarised Raman bands (*A*-class) from weakly-polarised neighbours.

6.1.3. Fermi resonance and resonance Raman scattering

Although the theory predicts that the depolarisation ratio (ρ_{iso}) of an isotropic sample should be in the range of $0 \leq \rho_{iso} \leq 3/4$, a ρ_{iso} value over 3/4 might be measured in practice [73, 74]. Fermi resonance [27] could be responsible for this observation, where a set of Raman bands with similar vibrational energies resonate and degenerate with each other.

Resonance Raman scattering could also cause such degeneracy [75] due to the interaction between vibrational and electronic energy transitions. In this case, the ρ_{iso} value may change with respect to the frequency of excitation laser; hence it is possible to identify the resonant band by measuring the ρ_{iso} value with different laser sources. Nevertheless, it is of importance to ensure that these resonance effects should not disturb the Raman band chosen for the molecular orientation study.

6.1.4. Fluorescence background

It may happen that the Raman scattering peaks are hidden by a strong fluorescent background [28], which reduces the S/N ratio of the spectra. This fluorescence is normally caused by impurities in the sample, and thus the primary solution is to prepare a sample with high purity. The photo-bleaching technique [76] is also useful to reduce the fluorescence background, although it takes time and there is a risk of sample degradation during the exposure. Owing to the difference in the time scale between Raman scattering (order of picosecond) and fluorescence (order of nanosecond), a time-resolved gated detector [28] can collect the Raman spectra separated from fluorescence.

An alternative approach to avoid the fluorescence is to use different laser sources, particularly with higher frequencies such as near IR or Nd:YAG laser sources, where the Raman excitation occurs outside the absorption of fluorescent materials. Apart from the use of conventional Raman equipment, a Fourier-transfer Raman spectrometer can increase the S/N ratio. Combined with a statistical analysis [77], the Raman scattering intensity can be determined more precisely.

6.2. Sample geometry

6.2.1. Multiple Raman scattering

Optical discontinuity [78] at the interface between the sample and the environment causes refraction and scattering [73] of the polarised light, which results in the

scrambling of the polarisation. As a consequence, it has been observed that the orientation coefficients showed disagreement between different techniques [71]. Some studies successfully reduced the influence of the optical discontinuity by immersing or by embedding the sample in a medium for which the refractive index is comparable to the index of the sample [14, 79–82].

The clarity of the sample is also important to avoid scrambling of the incident and scattered beams [83, 84]. This scrambling sometimes causes experimental difficulties in highly-crystalline translucent samples [85].

6.2.2. Sample thickness

A change in the depolarisation ratio with respect to the thickness of the sample has been observed for some materials [73, 80, 86]. This kind of phenomenon is often due to the difference in scattering volume (Raman cross-section) of the sample for each measurement. One solution is to measure the depolarisation ratio of specimens with different thickness and to extrapolate the ratio to zero thickness [53, 86].

6.2.3. Sample birefringence

The birefringence of the sample is also considered to affect the Raman scattering such as by increasing the irradiation volume of the sample [87] or by causing polarisation scrambling [72, 88]. One study [89] also discussed the possibility of polarisation scrambling due to the small residual stresses in non-oriented samples. The effect of birefringence on Raman scattering has been discussed in detail in references [23, 24, 53, 55, 78, 80, 90], which consider reflectivity and internal field corrections. According to Everall [55], the Raman intensity observed (I_{ij-obs}) can be treated with two parameters in terms of reflectivity (C_R) and internal field (C_{IF}) to calculate the corrected Raman scattering intensity ($I_{ij-R,IF}$) by:

$$I_{ij-R,IF} = C_R C_{IF} I_{ij-obs} \quad (80)$$

where the incident and scattered beams are polarised in the i and j directions, respectively, and each parameter is correlated with the refractive indices of the material along the i and j axes (n_i, n_j) as follows:

$$C_R = \frac{(n_i + 1)^2 (n_j + 1)^2}{[(n_i + 1)^2 - (n_i - 1)^2][(n_j + 1)^2 - (n_j - 1)^2]} \quad (81)$$

and,

$$C_{IF} = \frac{81n_i}{n_j (2 + n_i^2)^2 (2 + n_j^2)^2} \quad (82)$$

In fact, the study by Everall [55] showed empirically that PET fibres with a birefringence difference of 0.061 resulted only in $\sim 5\%$ change in their $\langle \cos^2 \theta \rangle$ values. Therefore, it is unlikely that the effect of sample birefringence is critical for the study of molecular orientation. The effect of the birefringence could also be reduced by immersing into media [71] as mentioned in Section 6.2.1.

6.3. Instrumental factors

6.3.1. Divergence of the incident beam

For the accurate measurement of polarised Raman scattering intensity, it is essential for the incident laser beam to be highly polarised. The divergence of the incident beam used to influence the polarisation of the Raman scattering in combination with the birefringence effect [78]. Nowadays, however, the laser polarisation can be controlled well by a polarisation filter and a half-wave ($\lambda/2$) plate. The beam divergence can be corrected by considering [55] the refractive index of the sample along the direction of the analyser (n_j):

$$I_{ij-BD} = n_j^2 I_{ij-obs} \quad (83)$$

6.3.2. Scattering collection geometry

The polarisation scrambling is also dependent on the geometry of Raman scattering collection geometry, which varies in optical path length [91]. In the transmission collection geometry [73, 74, 76, 80, 92], the sample should be thin enough to minimise the intensity loss and polarisation scrambling of the Raman scattering within the sample. In the right-angle scattering (RAS) geometry, the focal point of the sample should be just below the surface for the same reasons [74]. In the back-scattering (BS) geometry, the effect of the polarisation scrambling is less troublesome owing to the small scattering volume [71, 76, 93]. Nevertheless, it is important to focus the incident beam at the surface of the sample [91].

As well as depending on the scattering volume, the polarised Raman scattering intensity is also dependent on the scattering collection angle [35], for which an intensity calibration is required for the RAS geometry while no such calibration is necessary for the BS geometry.

6.3.3. Dichroic response of the instrument

A beam splitter is usually employed to allow only Raman scattered light to pass but to prevent the incident beam and the Rayleigh scattered light from going to the spectral analyser. The reflection and transmission coefficients of the beam splitter depend on the polarisation of the beam and the wavelength of the incident beam [55, 91, 94, 95]. As a result, some of the depolarisation ratio measurements seemed to be affected by their beam splitters

[95, 96], although the influence seems to be suppressed successfully in modern instruments [91].

6.3.4. Effect of the objective lens

When the polarised Raman spectroscopy is combined with optical microscopy, the distortion of incident light and Raman scattering due to the objective lens may influence [91] the process of analysing polarised Raman scattering.

Previous studies by Turrell and co-workers [91, 97–99] considered the effect of objective lenses by measuring the depolarisation ratio of isotropic liquid and gas samples [98] and anisotropic single crystals [91, 98, 99]. Two reasons were considered [98] to be responsible for the polarisation leakage in Raman microscopy: (a) a conical geometry of the scattering volume and (b) the depolarisation effect of the microscope objective.

Experimental results of these studies showed that the depolarisation effect of the objective lens is small when the numerical aperture (N.A.) of the lens is small. This is considered [98] to be due to the fact that the conical scattering volume is more cylindrical when the lens with a smaller N.A. is used. Following the laboratory-axis coordinate defined in Fig. 6, incident light polarised in the Z_L axis is distorted by the objective lens, and induces an X_L -axis component when the light is focused on the sample. The higher the numerical aperture, the higher the angle of focus; hence the more the amount of the induced X_L -axis component. Therefore, the use of a small N.A. objective lens would reduce the scattering due to the induced X_L -axis component of the light. According to their calculation [98], the depolarisation ratio of a perfectly-polarised and depolarised Raman band would be expected to be 0.77 and 0.135 using an objective lens ($\times 160$) with a N. A. value of 0.95, despite the theory of Raman spectroscopy predicting these values to be 0.75 and 0, respectively.

For an isotropic sample, no apparent effect due to the objective lens of $\times 50$ was observed [91, 99] with lenses up to N.A. = 0.85. For a sample with anisotropy, on the other hand, a study [91] showed that sample birefringence could influence the polarised Raman scattering by measuring the depolarisation ratio of an α -quartz single crystal. When the optical axis of the crystal was perpendicular to the propagation of the incident light, a negligible effect of the objective lens was observed for lenses with N.A. up to 0.85. However, the limit of N.A. was lowered to 0.63 when the optical axis of the crystal was aligned in the direction parallel to the propagation direction of the incident light. The study suggested that the effect due to the sample birefringence could be reduced by shortening the optical path within the sample.

On the other hand, another study [84] also showed a correlation of the focal length of the objective lenses and

the Raman scattering intensity in respect of the clarity of the sample. By utilising an optical fibre with focal lengths of ~ 65 mm ($f/3$) and ~ 445 mm ($f/10$), an intensity reduction by $\sim 16\%$ was observed for a transparent sample with an $f/10$ lens, while the intensity declined by $\sim 73\%$ for an opaque sample.

Therefore, it is important to choose a suitable objective lens with a N. A. value which does not disturb the polarised Raman intensity measurements. It is also desirable to measure the depolarisation ratio of the Raman scattering intensity using lenses with different N. A. values [14].

6.3.5. Calibration of instrumental factors

As explained above, several external factors can affect the measurement of polarised Raman scattering. Although the influence of each factor may be small, their accumulation could cause considerable experimental error. Hence, it is recommended to calibrate the system sensitivity to a polarised laser beam prior to embarking upon polarised Raman studies. The calibration can be performed by measuring the relative transmission of white polarisation—scrambled light [95].

An alternative and easier way to calibrate the instrumental factors is to measure the depolarisation ratio of a substance for which the ratio is well known. Carbon tetrachloride (CCl_4) [63, 91, 94, 100] and a α -quartz single crystal [91, 94] are widely used for the intensity calibration. In the case of CCl_4 sample, the intense Raman bands at 459 cm^{-1} , 314 cm^{-1} and 220 cm^{-1} have been used in some studies [94, 101]. The band at 459 cm^{-1} is a symmetric ν_1 vibrational mode in the polarised A_1 class, and the depolarisation ratio has been reported as 0.003 [101]. However, different ρ values were reported in some papers [63, 95] probably due to experimental error in the evaluation of the weak I_\perp value. On the other hand, the bands at 314 cm^{-1} and 220 cm^{-1} are asymmetric ν_4 vibrational modes in the F_2 class [94], for which the depolarisation ratios should be 0.75. Therefore, it is recommended to use the 314 cm^{-1} and 220 cm^{-1} of CCl_4 bands for instrumental calibration. Assuming that the liquid CCl_4 is isotropic, the intensity of the Raman scattering (I_{ij}) for these bands can be calculated to be:

$$I_{YY} = I_{ZZ}, \quad I_{YZ} = I_{ZY} \quad (84)$$

and

$$\frac{I_{YZ}}{I_{ZZ}} = 0.75 \quad (85)$$

in the BS geometry.

7. Practical applications of polarised Raman spectroscopy for the study of molecular orientation distributions in polymers

In practice, a diversity of materials has been examined using polarised Raman spectroscopy for the evaluation of molecular orientation as well as for the assignment of vibrational modes and for conformational [102] and microstructural studies [103]. Studies on liquid crystals [17, 53, 86, 104, 105] have been performed widely since the molecules in these materials are highly oriented, which gives rise to a significant difference in the intensity of polarised Raman spectra. With regard to polymeric materials, a series of commodity polymers such as polyolefins, polyesters and poly(vinyl chloride) (PVC) have been of interest.

As described in Section 3.4, the symmetry of Raman tensors plays an important role in polarised Raman spectroscopy for the study of molecular orientation distributions. In addition, forms of the tensors depend not only on the vibrational modes of the molecules but also their conformation. Therefore, the following sections review previous studies of polarised Raman spectroscopy for a variety of materials, categorised by their types of molecular conformation.

7.1. Polymers with planar chain conformations

7.1.1. Polyethylene (PE)

Maxfield [79] firstly utilised the approach to evaluate molecular orientation in an oriented low density PE (LDPE) specimen. In the RAS geometry, the molecular orientation of crystalline phases and that of amorphous phases were measured, and they were correlated with the results of IR spectroscopy. Similar studies have been carried out by Pigeon *et al.* [74] and Citra *et al.* [93] on uniaxially-drawn high density PE (HDPE) specimens, and by Lu *et al.* [106] on extruded PE rods in both the RAS and BS geometries. Their findings were also compared with the data from X-ray diffraction [93, 106] and IR spectroscopy [106]. Interestingly, the study [106] successfully determined the local orientation of PE molecules in an extruded H-shape PE rod by employing polarised Raman microscopy. In terms of the correlation with macroscopic properties, Lu *et al.* [106] measured the relative Raman intensities of bands in high modulus PE fibres, and correlated them with their tensile moduli.

These molecular orientation studies have focused on the vibrational modes for which the principal axes of the polarisability tensors are coincident with the chain axis. On the other hand, Schlotter *et al.* [47] considered the orientation distribution of the polarisability tensor for which the principal axis lies perpendicular to the specimen drawing direction.

Finally, Nikolaeva *et al.* [48–50] introduced an alternative approach using polarised Raman spectroscopy for

the study in PE molecular orientation. In addition to the conventional technique based on the measurement of the absolute Raman scattering intensity dependent on the optical geometry, the intensity ratio of two specific Raman bands was employed for the evaluation of the degree of molecular orientation.

7.1.2. Poly(ethylene terephthalate) (PET)

A number of researchers have directed their attention to polyesters by applying polarised Raman spectroscopy, to PET in particular, owing to the industrial applications of the fibres. PET also gives strong, well-defined Raman spectra with a sharp intense peak at 1616 cm^{-1} , which has been assigned to the symmetric stretching vibrational mode of the phenylene ring. The polarisability tensor for this vibrational mode can be treated with cylindrical symmetry, and the ratios of the diagonal components have already been estimated [55, 69, 85, 96, 107, 108]. Furthermore, fibre specimens can be considered to have uniaxial orientation. Therefore, PET is one of the best examples of molecular orientation studies using this technique.

Probably because of the ease of the study, the morphologies of PET specimens have been often studied by the technique in parallel with the evaluation of the molecular orientation. To begin with, Derouault *et al.* [88] observed the molecular orientation in a PET sheet qualitatively in terms of the depolarisation ratio change through the film thickness direction. The RAS geometry was applied for his study, while the combination of the RAS and BS geometries enabled a series of investigations to be undertaken by Jarvis *et al.* [7], Nobbs *et al.* [22], Lewis *et al.* [71], and Purvis *et al.* [80, 107] on uniaxially- and biaxially-oriented PET specimens.

Raman microscopy was employed by Adar *et al.* [96] and by Rodriguez *et al.* [109] for qualitative molecular orientation analyses, which also considered crystallinity and the band width of the spectra [96]. Another qualitative study by Natarajan *et al.* [110] discussed the relation between relative Raman intensities and macroscopic properties such as birefringence and density. These Raman spectroscopic studies have been correlated by Laperonne *et al.* [23] with the other analytical methods such as NMR [8], IR spectroscopy, X-ray diffraction, and birefringence measurements. In the latter work [8], Ward discussed the molecular orientation in the crystalline and amorphous phases in detail. Huijts *et al.* [111] also employed both the Raman and birefringence techniques to the molecular orientation study of as-spun PET fibres and compared with poly(ethylene naphthalate) (PEN). Lesko *et al.* [66] and Michielsen and co-workers [60, 112, 113] studied the molecular orientation of a wide range of PET spun fibres and related it with their sample birefringence. Conventional Raman spectroscopy [55] and FT-Raman spectroscopy [114] have been also applied by Everall and

others for a series of uniaxially- and biaxially-oriented PET specimens to classify the samples with respect to their crystallinity and molecular orientation. Bower *et al.* [46] also studied biaxial orientation in PET films, and characterised molecular orientation using the most probable orientation distribution function.

7.1.3. Other materials with planar chain conformations

Apart from the extended research on PE and PET above, the molecular orientation of several other polymeric materials has been evaluated. Robinson *et al.* [13] targeted poly(vinyl chloride) (PVC) with moderate crystallinity for the study of the plasticising effect on the molecular orientation during drawing. The orientation distribution coefficients were determined based on the C–Cl stretching band, and it was concluded that the crystallinity declined during the drawing process.

Some of engineering polyesters and polyamides have also been studied, such as PEN [111], poly(ether ether ketone) (PEEK) [115], nylons [116]. These results were rather qualitative except for the study on PEN, for which the orientation distribution parameter $\langle \cos^2 \theta \rangle$ was obtained and correlated linearly with the result of birefringence measurements. Other types of aromatic polyesters [17, 117] have also been of interest since the symmetric stretching vibration of their phenylene ring gives intense Raman scattering. Molecular orientation in polysulfone hollow fibres was measured by Prokhorov *et al.* [50], and the study successfully related the result to their draw ratios in spite of a complicated sample geometry. Furthermore, the molecular orientation of polycarbonate (PC) in high-modulus carbon fibre/PC composite materials was measured [118] quantitatively to explain the deformation micromechanics of composite materials with a single fibre.

Similarly in fluorescence spectroscopy, polyene probes were used [119] to study the molecular orientation distributions in PE materials. Although the technique is an indirect measurement of the molecular chain orientation, the study showed the orientation distribution in the amorphous phases in the sample since the probes are thought to be adsorbed selectively to the amorphous phase.

7.2. Polymers with helical molecular conformations

7.2.1. Isotactic polypropylene (it.PP)

While FT-IR, X-ray diffraction, and birefringence measurement are regarded as common approaches for the study of molecular orientation distributions in it.PP materials [120, 121], relatively little research has been reported on orientation studies by means of polarised Raman spectroscopy. Apart from some qualitative studies [59, 85,

122] of molecular orientation, Satija *et al.* [14] evaluated the molecular orientation coefficients of a hydrostatically-extruded it.PP in the RAS geometry. Their observations were correlated successfully with the results derived from birefringence measurements and X-ray diffraction. On the other hand, Wang *et al.* [123] measured the molecular orientation coefficients of extruded PP rods. They compared the results with those obtained from Brillouin scattering, and further correlated these with the elastic constant of the material. Apart from these quantitative analyses, a number of researchers have applied polarised Raman spectroscopy to obtain molecular orientation information qualitatively. These studies focused on the deformation behaviour of amorphous and crystalline phases of it.PP films [59], the correlation between relative Raman intensities and birefringence of it.PP fibres [124], and the local orientation of it.PP matrix in an it.PP/CaCO₃ composite material [125]. In addition, Baez *et al.* [85] examined the applicability of FT-Raman to determine the molecular orientation of it.PP, although the study provided only qualitative information.

Recently, it.PP composite materials [126] have been introduced to enhance the mechanical properties of it.PP matrix by organic and inorganic fillers. The incorporation of the filler compounds can lead to trans-crystallisation [127] and preferential molecular orientation in the it.PP matrix [125, 128]. Polarised Raman spectroscopy has been applied to an it.PP composite with PET fibre reinforcement [127], and the study successfully revealed the trans-crystallisation between α - and β -form at filler/matrix interface. By comparing relative Raman intensities, preferential orientation of it.PP molecules was also observed, while similar results were obtained [125] for a CaCO₃/it.PP composite material. In the study [128] of a single-wall carbon nanotube (SWNT)/it.PP composite material, uniaxially-drawn specimens showed higher molecular orientation of SWNT fillers compared to the it.PP matrix.

It is of interest that the studies by Satija [14] and Wang *et al.* [123] have been the only successful cases of the quantitative measurement of molecular orientation of it.PP. In spite of the fact that it.PP provides relatively simple spectra that are similar to PE, additional considerations are necessary due to its helical conformation.

7.2.2. Other conventional polymers with helical chain conformations

Although the spectroscopic technique has been applied to a number of helical molecules, only two polymers have been investigated using a similar approach to it.PP. Purvis *et al.* [81] reported the orientation distribution coefficients of a uniaxially-oriented poly(methyl methacrylate) (PMMA) specimen, and the observations were related to the results of birefringence measurements and NMR [129]. They also pointed out that the molecule had

a helical conformation since it was reasonable to assume the cylindrical symmetry of the polarisability tensor. The other example was atactic PS (at.PS) studied by Jasse and co-workers [100, 130]. In addition to the assignment of the vibrational modes, they evaluated the molecular orientation in a uniaxially stretched at.PS, for which $\langle \cos^2 \theta \rangle$ agreed well with the result from IR dichroism [100].

Polarised Raman spectroscopy has been used for vibrational mode assignment and the qualitative measurement of molecular orientation in poly(tetrafluoroethylene) copolymers [131, 132]. A compostable polymer, poly(L-lactic acid) is another example of helical polymers. Polarised Raman spectra were obtained [133, 134], and the Raman band positions were found to shift depending on the molecular orientation. The study [134] also evaluated the molecular orientation in a PLLA film qualitatively by means of relative intensity measurements.

7.2.3. Polymers of biological origins

As well as synthetic polymers, molecular orientation distributions in polymers of biological origins have been of interest recently in order to study their microstructures and relate them to their macroscopic properties. With regards to the application of polarised Raman spectroscopy, some studies [135–137] focused on the orientation distributions of chromophores and proteins in filamentous macromolecular assemblies such as viruses. By measuring Raman intensities in the BS geometry, uniaxial orientation of the helical backbone units was evaluated quantitatively.

More recently, the technique was applied for the study of molecular orientation distributions in silk fibres [138]. It was shown that the orientation distributions of β -sheet structural units are unique between different silk fibres, which would be correlated with their macroscopic mechanical properties. The study also referred to the tilt angle of the peptide C=O group, and concluded that the direction of this functional group is nearly perpendicular to the chain axis.

Apart from the study of molecular orientation distributions, polarised Raman spectroscopy plays an important role in the determination of the molecular structure, which could be particularly useful in biological and medical fields. Based on the analysis of well-oriented specimens, the tilt angle of a specific vibrational mode could provide information about the orientation of the functional group in the molecule. This technique has been applied for the helical chain orientation in poly(L-alanine) [139] and subunits in a filamentous virus [140].

8. Case study: Molecular orientation distributions in uniaxially-oriented PET fibres

As reviewed in the previous sections, a number of studies have already established the theoretical background of the analysis of molecular orientation by means of polarised

Raman spectroscopy. However, a practical example needs to be given of the process to determine the molecular orientation distribution coefficients. In this section, the molecular orientation distribution of PET materials was studied in order to review the validity of the technique and the factors influencing their measurement.

8.1. Background

The molecular orientation of PET materials has been studied widely as summarised in Section 7.1.2. The Raman band at 1616 cm^{-1} has been regarded as an ideal peak for the studies of molecular orientation. This band gives a sharp, intense Raman scattering as shown in Fig. 9, and the ρ_{iso} value was reported to be 0.5484 [107]. The ratio of the diagonal Raman tensors (a_{xx} , a_{yy} , a_{zz}) was also determined as $a_{xx} \approx a_{yy}$, $a_{xx}/a_{zz} = -0.18$ [80, 107]. In the current study, uniaxially-oriented PET fibres were employed since only the P_{100} values are non-zero for a specimen with uniaxial orientation (Section 4.1), which can reduce the number of parameters that have to be determined.

This section also includes the process of the system calibration, and the molecular orientation distribution coefficients are discussed with reference to the birefringence and tensile modulus of the specimen.

8.2. Experimental

Four types of uniaxially-oriented PET fibre specimens [141] were supplied by Akzo Nobel. Their birefringence and mechanical properties are listed in Table IV. The birefringence was determined as an average of the measurement for 10 single filaments under a polarised optical microscope fitted with a Senarmont compensator. The mechanical properties of each specimen were deter-

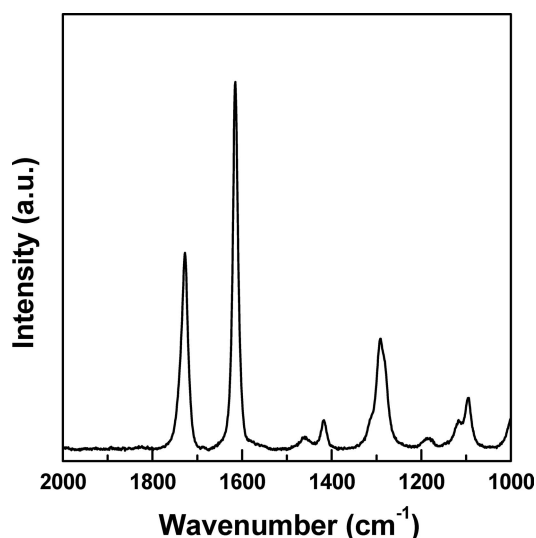


Figure 9 Polarised Raman spectra of PET fibre specimen PR for the $X_L(Z_L Z_L)X_L$ scattering geometry.

TABLE IV Sample birefringence (Δn) and mechanical properties of the PET fibre specimens

Code [141]	Δn (-)	Tensile modulus (GPa)	Tensile strength (MPa)	Elongation at break (%)
PC	0.180 ± 0.004	17.5 ± 0.6	922 ± 54	12.1 ± 1.8
PL	0.167 ± 0.004	17.2 ± 0.8	749 ± 28	16.8 ± 1.7
PM	0.192 ± 0.005	18.5 ± 0.7	1042 ± 65	10.9 ± 1.2
PR	0.171 ± 0.013	15.8 ± 0.7	687 ± 20	13.5 ± 0.7

mined from averaging 20 replicated measurements using a mechanical testing machine (Instron 1121) with an initial sample gauge length of 50 mm and a strain rate of 10%/min. For polarised Raman spectroscopy, a single filament of each specimen was mounted across an O-ring washer.

A Raman microscope (System 1000, Renishaw) equipped with a HeNe laser ($\lambda = 632.8$ nm, output 26 mW) was used for the measurement of polarised Raman scattering intensity. The incident laser beam was focused at the surface of the sample, and the Raman scattering was collected with an objective lens ($\times 50$, N.A. = 0.75) in the BS geometry. The PET sample was aligned with its fibre axis parallel to the Z_L laboratory axis (Fig. 6). Special care was taken so that the CCl_4 vapour did not affect the Raman scattering collection. The Raman shift was calibrated with the peak [142] at 521 cm^{-1} of a Si standard (Renishaw).

The Raman scattering intensity was measured for three combinations of the polarisation direction of the incident beam and the Raman scattering, i.e. $X_L(Z_L Z_L)X_L$, $X_L(Y_L Z_L)X_L$, and $X_L(Y_L Y_L)X_L$, using polarisation filters and a half-wave ($\lambda/2$) plate. The observed intensity was corrected for the polarisation sensitivity of the instrument, the effect of the sample birefringence (Section 6.2.3) and the divergence of the incident beam (Section 6.3.1), assuming that the averaged refractive index (n_{av}) of PET [80] was 1.58, which is related [68] to the refractive indices parallel (n_e) and perpendicular (n_o) to the fibre axis by,

$$n_{av} = \frac{n_e + 2n_o}{3} \quad (85)$$

The P_{100} values were obtained from the set of the polarised Raman scattering intensity measurements according to the procedure described in Section 3.9. The expansion coefficients $A_{100}^{g'g'p'p}/a_{zz}^2$ were calculated using the ratios of the Raman tensor components [80, 107], and are listed in Table V.

8.3. Results

8.3.1. System calibration with CCl_4

Prior to the measurement of polarised Raman scattering intensity of the PET fibre specimens, the polarisation sen-

TABLE V Expansion coefficients ($A_{100}^{g'g'p'p}/a_{zz}^2$) for the 1616 cm^{-1} Raman band of the PET fibre specimens

$\alpha_{g'g'p'p}^2$	A_{000}/a_{zz}^2	A_{200}/a_{zz}^2	A_{400}/a_{zz}^2
α_{XX}^2	0.2394	-0.1621	5.626×10^{-2}
α_{ZZ}^2	0.2394	0.3241	0.1500
α_{ZX}^2	0.1313	4.193×10^{-2}	-7.502×10^{-2}

sitivity of the system was calibrated with CCl_4 (99%, BDH). Liquid CCl_4 was kept in an open glass vial for the whole of the experiment.

Fig. 10 shows polarised Raman spectra of CCl_4 with respect to $X_L(Z_L Z_L)X_L$, $X_L(Y_L Z_L)X_L$, and $X_L(Y_L Y_L)X_L$ polarisation geometries. Three peaks were observed at around 460 cm^{-1} , 320 cm^{-1} and 225 cm^{-1} . The Raman scattering intensity of the band at 460 cm^{-1} was reduced significantly in the $X_L(Y_L Z_L)X_L$ geometry, which indicates that the band belongs to the A-class (polarised, $\rho_{iso} < 0.75$) which agreed with references [63, 91, 94]. On the other hand, the bands at 320 cm^{-1} and 225 cm^{-1} should be the F-class (depolarised, $\rho_{iso} = 0.75$) according to the references. Since the peak at 225 cm^{-1} was asymmetric probably due to the influence of Rayleigh scattering background, the peak at 320 cm^{-1} was more reliable and used for the instrumental calibration for polarised Raman scattering intensity measurement. The instrumental correction described in Section 6.3 was assumed that the CCl_4 sample was isotropic, which gave the intensity correction factors of 1.08 and 0.92 for the $X_L(Y_L Z_L)X_L$, and $X_L(Y_L Y_L)X_L$ geometries. Therefore, the polarised Raman scattering intensities in these geometries were multiplied by these values prior to the calculation of the P_{100} values.

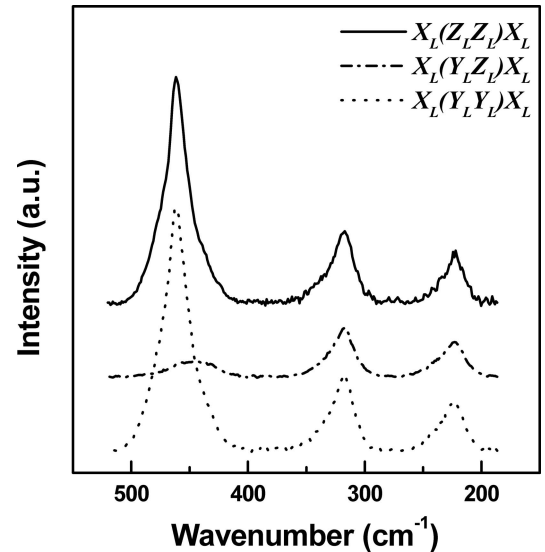


Figure 10 Polarised Raman spectra of CCl_4 for different scattering geometries.

8.3.2. Molecular orientation distribution coefficients of PET fibres

Polarised Raman spectra of specimen PR with different polarisation combinations are shown in Fig. 11. A unique response was observed for each Raman band for each of the polarisation directions of the incident beam and the analyser, which was caused by the direction and the magnitude of the Raman tensor components as well as the orientation distribution of the orienting unit. Focusing on the band at 1616 cm^{-1} , the peak height of the scattering was measured and used for the determination of the P_{100} values. The set of intensities were summarised for each specimen in Table VI, which was normalised to the intensity in the $X_L(Z_L Z_L)X_L$ geometry.

As given in Table VII, the P_{100} values were calculated referring to Equations 13 and 31 assuming that the principal axis of the Raman tensor was parallel to that of the orienting unit. Fig. 12 shows the correlation between the P_{200} and P_{400} values, in which the boundaries to classify the molecular orientation distribution (Fig. 8) have been superposed. All specimens were found to have a monotonic increase in molecular orientation distribution toward the fibre axis.

As mentioned briefly in the introductory part of this review, the P_{200} value can be correlated with the birefrin-

TABLE VI Ratio of the Raman scattering intensity at 1616 cm^{-1} of the PET fibre specimens collected in different scattering geometries ($I_{X_L(Z_L Z_L)X_L} = 100$)

Code [141]	$I_{X_L(Z_L Z_L)X_L}$	$I_{X_L(Y_L Z_L)X_L}$	$I_{X_L(Y_L Y_L)X_L}$
PC	100	14.3 ± 0.3	9.2 ± 0.1
PL	100	17.2 ± 2.0	10.8 ± 0.2
PM	100	13.9 ± 0.4	6.8 ± 0.2
PR	100	15.0 ± 0.3	9.2 ± 0.2

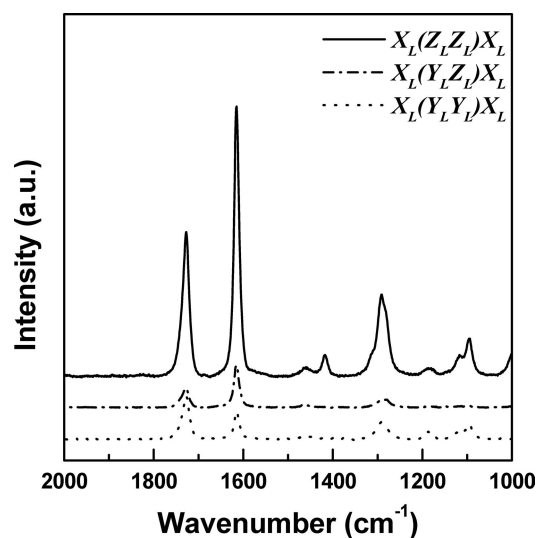


Figure 11 Polarised Raman spectra of PET fibre specimen PR for different scattering geometries.

TABLE VII Molecular orientation distribution coefficients (P_{100}) of the PET fibre specimens

Code [141]	P_{200}	P_{400}
PC	0.600 ± 0.004	0.316 ± 0.008
PL	0.557 ± 0.003	0.263 ± 0.003
PM	0.650 ± 0.007	0.324 ± 0.012
PR	0.596 ± 0.005	0.298 ± 0.005

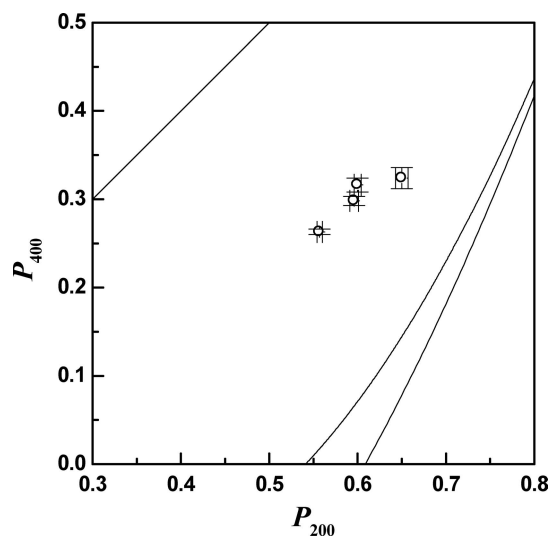


Figure 12 Relationship between the P_{200} and P_{400} values of the PET fibre specimens determined by polarised Raman spectroscopy.

gence (Δn) of the sample [68] by,

$$\Delta n = P_{200} \Delta n_{\max} \quad (87)$$

where Δn_{\max} is a intrinsic birefringence of the material. The P_{200} value determined by polarised Raman spectroscopy ($P_{200, C1-C4}$) was related to the sample birefringence in Fig. 13. Although the plots were scattered due to a similarity in the molecular orientation distribution between the samples, a linear trend line through the origin gave a Δn_{\max} value of 0.296 ± 0.003 at the intercept to $P_{200} = 1$. This Δn_{\max} value is large compared with the value around 0.24 reported in the previous studies [70, 78, 107, 111, 143]. This discrepancy could be explained by considering the tilt angle (Section 6.1.1) as follows.

The P_{200} value for the 1616 cm^{-1} Raman band, in fact, represents the orientation distribution of the principal axis of the Raman tensor. In order to obtain the P_{200} value for the molecular chains ($P_{200, \text{chain}}$), the P_{200} value needs to be corrected for the tilt angle. The Raman band at 1616 cm^{-1} of PET was assigned [80, 108, 144] to the symmetrical stretching vibration along the C_1-C_4 direction of its phenylene ring, in which the principal axis of the Raman tensor is tilted for about 19° from the molecular chain direction [107, 145]. Therefore, an angular correction was required to obtain the orientation distribution coefficients

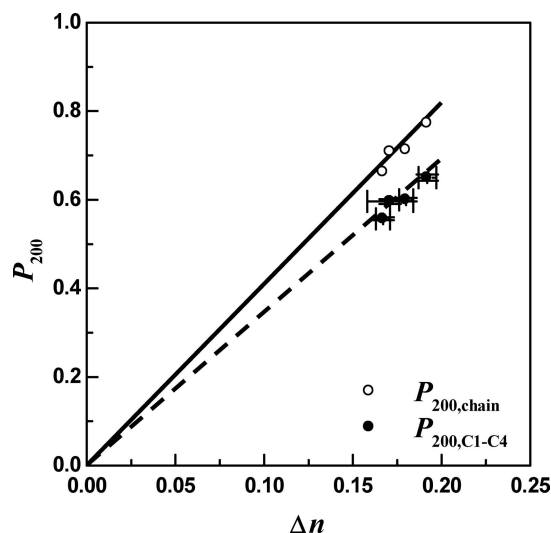


Figure 13 Relationship between sample birefringence and the values of $P_{200,C1-C4}$ and $P_{200,chain}$ for the PET fibre specimens.

of PET molecules in the sample. Using Equation 79, the P_{200} values for the molecular chains ($P_{200,chain}$) of the PET specimens were calculated from those for the $P_{200,C1-C4}$ values. The results are also shown in Fig. 13, and the Δn_{max} value was obtained to be 0.249 ± 0.003 , which is consistent with the reference values around 0.24.

8.3.3. Molecular orientation distribution function: $N(\theta)$ and $N_{mp}(\theta)$

Similar to the $P_{200,chain}$ value, the $P_{400,chain}$ value can be determined from the P_{400} value using Equation 79. Using these $P_{200,chain}$ and $P_{400,chain}$ values, it is possible to obtain their molecular orientation distribution functions $N(\theta)$ according to Equation 36.

In Fig. 14, the function $N(\theta)$ is shown for specimen PM, which gave the highest P_{200} value of all the specimens. The function $N(\theta)$ increases as the angle θ is close to 0° . This indicates that the molecular chains are more oriented toward the fibre axis. On the other hand, there was a negative region of the function $N(\theta)$ between 44° to 72° . In addition, the distribution is shown to be bimodal with two maxima at $\theta = 0^\circ$ and 90° , which is unlikely to present in the specimen studied here. These unrealistic observations are considered as errors due to the P_{100} values for the order l higher than 6 to be included in Equation 36. As shown in the same figure, these errors are improved by introducing the most probable molecular orientation distribution function $N_{mp}(\theta)$ in Equation 77.

Fig. 14 also shows the function $N(\theta)$ where only the P_{200} value is taken into account. This function corresponds to the study of molecular orientation distributions by birefringence measurement or IR dichroism measurement. The function $N(\theta)$ is much broader, as it may be subject

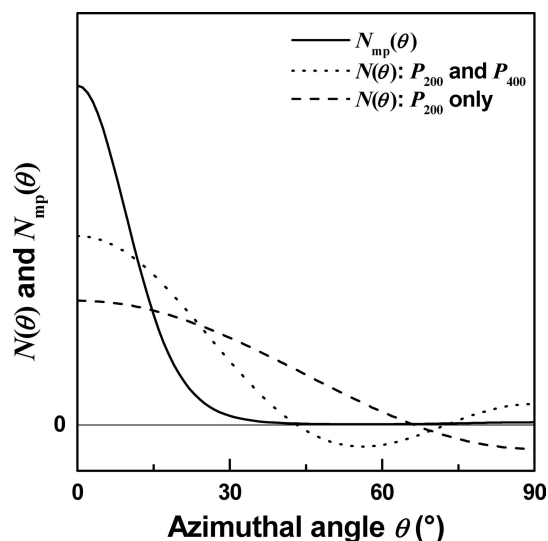


Figure 14 Comparison of molecular orientation distribution functions $N(\theta)$ and $N_{mp}(\theta)$; PET fibre specimen PM.

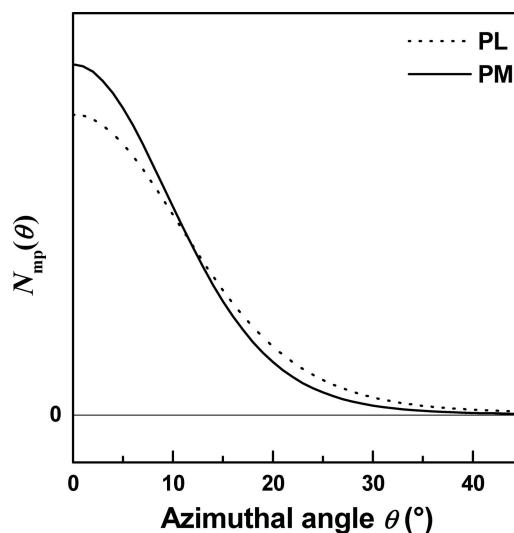


Figure 15 Comparison of the function $N_{mp}(\theta)$; PET fibre specimens PL and PM.

to a large error since the function ignores all the high order coefficients except for the P_{200} value in Equation 36.

Finally, the difference in molecular orientation distributions between different PET fibres is compared with respect to their functions $N_{mp}(\theta)$. For clarity, the samples giving the highest and lowest P_{200} values (PM and PL, respectively) were chosen, and their functions $N_{mp}(\theta)$ are shown in Fig. 15. The function $N_{mp}(\theta)$ of specimen PM gives a higher and narrower maximum at $\theta = 0^\circ$ than that of specimen PL. This clearly indicates that the specimen PM has higher molecular orientation than specimen PL.

The analysis above demonstrates that the function $N(\theta)$ is useful to visualise the molecular orientation distributions in the sample. Polarised Raman spectroscopy, which enables to determine orientation coefficients up to P_{4mn}

values, was shown to improve the accuracy of the function $N(\theta)$. Furthermore, the errors due to the lack of information about P_{lm} values for $l \geq 6$ would be reduced by introducing the function $N_{mp}(\theta)$.

8.3.4. Correlation between molecular orientation distribution and macroscopic tensile properties

The microstructure of a material such as molecular orientation is known to have a large effect upon its macroscopic mechanical characteristics. In relation to the molecular orientation distribution coefficients, the tensile modulus has contributions from both $\langle \cos^2 \theta \rangle$ and $\langle \cos^4 \theta \rangle$ values [146, 147], which are derived from the P_{200} and P_{400} values using Equations 68 and 69.

Assuming a Reuss-type aggregate model [148], the tensile compliance along the fibre axis, $\langle s_{33} \rangle$, which is the reciprocal of the tensile modulus is described as,

$$\begin{aligned} \langle s_{33} \rangle = & s_{11} \langle \sin^4 \theta \rangle + s_{33} \langle \cos^4 \theta \rangle \\ & + (2s_{13} + s_{44}) \langle \sin^2 \theta \cos^2 \theta \rangle \end{aligned} \quad (88)$$

where s_{ij} are compliance matrix components. The values of $\langle \sin^4 \theta \rangle$ and $\langle \sin^2 \theta \cos^2 \theta \rangle$ are obtained using,

$$\langle \sin^4 \theta \rangle = 1 - 2 \langle \cos^2 \theta \rangle + \langle \cos^4 \theta \rangle$$

$$\langle \sin^2 \theta \cos^2 \theta \rangle = \langle \cos^2 \theta \rangle - \langle \cos^4 \theta \rangle$$

Since the molecules are considered to be highly oriented along the fibre direction considering the P_{100} values obtained, some approximations were made to simplify Equation 88. Firstly, the s_{11} value was equal to the s_{44} value, and the s_{13} value was very small compared to the s_{44} value. Secondly, the s_{11} and s_{33} values were calculated to be 2.5×10^{-10} and $0.1 \times 10^{-10} \text{ m}^2/\text{N}$, respectively, based on the elastic moduli of the crystalline phases of PET in the direction parallel [149] and perpendicular [150] to the chain direction. The calculated specimen modulus (E_{calc}) was consistent with that (E_{obs}) obtained from mechanical testing of the specimen as shown in Fig. 16. The results presented show that polarised Raman spectroscopy could be useful for the prediction of mechanical properties of materials.

8.4. Summary

This section demonstrated the evaluation of molecular orientation distribution by means of polarised Raman spectroscopy. An example was given of CCl_4 being used for the calibration of the polarisation sensitivity of the instrument. The molecular orientation distribution coefficients (P_{l00}) were obtained for a series of uniaxially-oriented

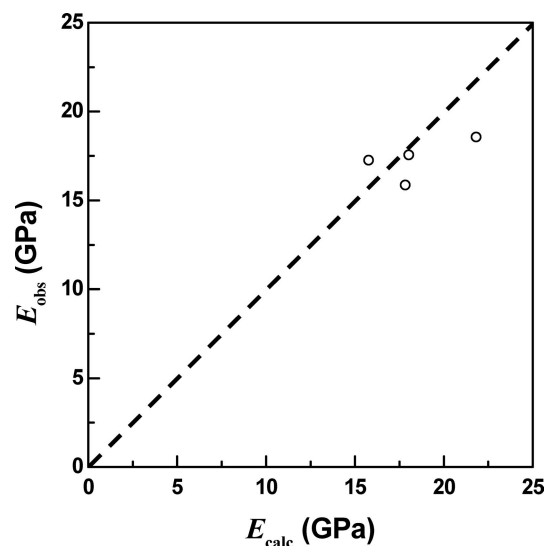


Figure 16 Comparison of tensile modulus (E_{calc}) of PET fibre specimens calculated from the P_{100} values determined by polarised Raman spectroscopy and that (E_{obs}) measured experimentally. (Dashed line: $E_{\text{calc}} = E_{\text{obs}}$).

PET fibres by measuring three polarised Raman scattering intensities with different polarisation combinations in the BS geometry.

The P_{200} values of the specimens were reasonably correlated with their sample birefringence, which gave a Δn_{max} value of 0.249 ± 0.003 for a sample with perfect orientation ($P_{200} = 1$). The molecular orientation distribution parameters $\langle \cos^2 \theta \rangle$ were derived from the P_{100} values for the purpose to predict the specimen modulus of the samples. With the approximations of the compliance matrix components for a highly oriented PET material, the E_{calc} values agreed with the experimental values of Young's modulus.

Two important points need to be taken into consideration to determine the P_{100} values. Primarily, the influence of birefringence on polarised Raman scattering intensity was not negligible for the samples with high birefringence. Secondly, the P_{100} values needed to be corrected for the tilting angle if the principal axis of orienting units is not coincident with the molecular chain axis since the Raman band intensity depends on the orientation of the structural units.

9. Conclusions

The properties of polymers vary as a consequence of their macro- and microscopic structures unique to the long chain molecules. The chemical characteristics of the material are determined mainly by the primary structure of the molecule, whereas the microstructure plays an important role on the physical characteristics. As seen in crystalline and amorphous materials, the degree of molecular orientation can be regarded as one of the most crucial parameters defining the macroscopic properties of the material.

The quantitative evaluation of molecular orientation is of great interest, and it can be expressed clearly in terms of the orientation distribution coefficients, P_{lmn} , or parameters, $(\cos^l \theta)$. The parameters are termed as the direction cosines of the angle between molecular chain direction and the principal axis of the sample, which is averaged over the volume in focus. Among several techniques to determine these coefficients and parameters, polarised Raman spectroscopy was focused upon and reviewed in detail in this paper. This method employs the inelastic scattering nature of polarised light as a result of the interaction with the induced dipole moment of the molecule. This spectroscopic approach has a number of advantages; first of all it is a non-destructive method and has no restriction on the sample shape. The orientation information can be obtained from amorphous phases as well as crystalline phases. Furthermore, the localised orientation on a scale of a few microns could be determined by combining with microscopic techniques.

The second and fourth orders of the orientation distribution coefficients can be determined by using polarised Raman spectroscopy. As shown in the example, this enables the technique to determine the molecular orientation distribution function, $N(\phi, \theta, \psi)$, more precisely than with the other techniques. In addition, the function can be further improved by introducing the most probable distribution function, $N_{mp}(\phi, \theta, \psi)$. For the majority of physical properties, their anisotropy can be related to the P_{2mn} values, while some mechanical properties such as Young's modulus are also related to the P_{4mn} values. The achievement of the higher order parameters is another strength of the polarised Raman spectroscopic technique for the precise understanding of the correlation between microstructure and the macroscopic characteristics of the material.

In spite of the usefulness of the method, its practical applications have been limited to a few specific materials such as polyethylene and PET, for which the molecular structures are relatively simple and which polarisability tensors were already known. On the other hand, the potential of the technique is still wide open for the other conventional polymers and need to be investigated, in conjunction with the alternative analytical techniques.

Such studies could range from commodity plastics to biodegradable polymers or even high performance polymer fibres. It should be possible for microscopic observation to characterise the local molecular orientation in materials moulded into complex shapes. Finally, the effect of molecular orientation on the physical properties can be explained precisely by polarised Raman spectroscopy owing to its capability of obtaining both P_{2mn} and P_{4mn} values.

Acknowledgement

The work was supported by the Four Square, A Division of Mars U.K. Ltd. One of the authors (MT) is grateful

to Universities UK for financial support through the ORS scheme (ORS/2000028028).

Appendix: Information entropy theory for the determination of the most probable molecular orientation distribution function

The original concept of the information theory was established by Shannon and co-workers [151, 152] in order to code messages with efficiency for the development of communication technology [153]. The concept was based on the frequency of alphabetical symbols used in the messages, "The more improbable the symbol, the greater the information". If the probability of a symbol (i) is given by p_i , the self information which the symbol i is defined as,

$$\log \frac{1}{p_i} \text{ or } -\log p_i$$

where the sum of the probabilities of all the symbols (of number M) should be unity, i.e.,

$$\sum_{i=1}^M p_i = 1$$

When a very large number of symbols N_S is used in a message, the number of symbols i in the message will be $N_S p_i$, and thus their information is given by

$$-N_S p_i \log p_i$$

and the average information per symbol, H , is given by,

$$\begin{aligned} H &= \frac{1}{N_S} \sum_{i=1}^M (-N_S p_i \log p_i) \\ &= -\sum_{i=1}^M p_i \log p_i \end{aligned} \quad (89)$$

which is the so-called *Shannon's information uncertainty*.

Shannon's theory was applied by Jaynes [154] to Gibb's canonical distribution theorem. According to the theory, the optimum energy of the system is to be chosen to maximise their information uncertainty [153], i.e. to maximise their entropy [155], if only partial information of the system is known. In other words, under constraints of partly-known information, the rest of unknown parts should be chosen for the H value in Equation 89 to be a minimum.

The information entropy theory of Jayne was employed further by Berne *et al.* [42], Pottel *et al.* [43] and Labarthe [44] in order to obtain the orientation distribution function $N(\theta)$ from the system giving a limited number of the coefficients P_{lmn} . The information entropy of the distribution

function $S[N(\phi, \theta, \psi)]$ is given [42–44] by,

$$S[N(\phi, \theta, \psi)] = - \int_0^\pi \int_0^{2\pi} \int_0^{2\pi} N(\phi, \theta, \psi) \ln N(\phi, \theta, \psi) d\psi d\phi d\theta \quad (72)$$

under the following constraints,

$$N(\phi, \theta, \psi) \geq 0 \quad (73)$$

and

$$\int_0^\pi \int_0^{2\pi} \int_0^{2\pi} N(\phi, \theta, \psi) \sin \theta d\psi d\phi d\theta = 1 \quad (74)$$

References

1. L. E. ALEXANDER, in "X-ray Diffraction Methods in Polymer Science" (Wiley-Interscience, John Wiley & Sons, Inc., New York, 1969).
2. H. KAWAI, S. NOMURA, I. KIMURA and M. KAGIYAMA, *J. Polym. Sci.: Part A-2* **8** (1970) 383.
3. A. H. WINDLE, in "Measurement of Molecular Orientation and Structure in Non-Crystalline Polymers by Wide Angle X-Ray Diffraction", in "Developments in Oriented Polymers-1", edited by I. M. WARD (Applied Science Publishers, London, 1982).
4. P. LAPPERSONNE, J.-F. TASSIN, L. MONNERIE and J. BEAUTEMPS, *Polym.* **32** (1991) 3331.
5. A. CUNNINGHAM, G. R. DAVIES and I. M. WARD, *ibid.* **15** (1974) 743.
6. A. CUNNINGHAM, I. M. WARD, H. A. WILLIS and V. ZICHY, *Polym.* **15** (1974) 749.
7. D. A. JARVIS, I. J. HUTCHINSON, D. I. BOWER and I. M. WARD, *Polym.* **21** (1980) 41.
8. I. M. WARD, in "Determination of Molecular Orientation by Spectroscopic Techniques", in "Advances in Polymer Science", edited by H. H. KAUSCH and H. G. ZACHMANN (Springer-Verlag, Berlin, 1985).
9. R.-J. ROE, *J. Polym. Sci.: Part A-2* **8** (1970) 1187.
10. V. J. MCBRIERTY and I. M. WARD, *Brit. J. Appl. Phys.* **1** (1968) 1529.
11. N. J. CLAYDEN, J. G. EAVES and L. CROOT, *Polym.* **38** (1997) 159.
12. M. BOTEV, R. NEFFATI and J. RAULT, *Polym.* **40** (1999) 5227.
13. M. E. R. ROBINSON, D. I. BOWER and W. F. MADDAMS, *J. Polym. Sci.: Polym. Phys. Ed.* **16** (1978) 2115.
14. S. K. SATIJA and C. H. WANG, *J. Chem. Phys.* **69** (1978) 2739.
15. D. Y. YOON, C. CHANG and R. S. STEIN, *J. Polym. Sci.: Polym. Phys. Ed.* **12** (1974) 2091.
16. V. PETRACCONE, I. C. SANCHEZ and R. S. STEIN, *J. Polym. Sci.: Polym. Phys. Ed.* **13** (1975) 1991.
17. G. VOYIATZIS, G. PETEKIDIS, D. VLASSOPOULOS, E. I. KAMITSOS and A. BRUGGEMAN, *Macromolecules* **29** (1996) 2244.
18. J. H. NOBBS, D. I. BOWER, I. M. WARD and D. PATTERSON, *Polym.* **15** (1974) 287.
19. F. PINAUD, J. P. JARRY, PH. SERGOT and L. MONNERIE, *ibid.* **23** (1982) 1575.
20. P. LAPPERSONNE, J. F. TASSIN, P. SERGOT, L. MONNERIE and G. BOURVELLEC, *ibid.* **30** (1989) 1558.
21. A. ELLIOTT, in "Infra-red Spectra and Structure of Organic Long-chain Polymers" (Edward Arnold, London, 1969).
22. J. H. NOBBS, D. I. BOWER and I. M. WARD, *J. Polym. Sci.: Polym. Phys. Ed.* **17** (1979) 259.
23. P. LAPPERSONNE, D. I. BOWER and I. M. WARD, *Polym.* **33** (1992) 1266.
24. D. I. BOWER, *J. Polym. Sci.: Polym. Phys. Ed.* **10** (1972) 2135.
25. C. V. RAMAN and K. S. KRISHNAN, *Nature* **121** (1928) 501.
26. J. J. LASERNA (ed.) in "Modern Techniques in Raman Spectroscopy" (John Wiley & Sons, Chichester, 1996).
27. C. N. BANWELL and E. M. MCCASH, in "Fundamentals of Molecular Spectroscopy" (The McGraw-Hill Companies, London, 1994).
28. J. L. KOENIG, in "Spectroscopy of Polymers" (Elsevier, Oxford, 1999).
29. H. J. BOWLEY, D. J. GARDINER, D. L. GERRARD, P. R. GRAVES, J. D. LOUDEN and G. TURRELL, in "Practical Raman Spectroscopy" (Springer-Verlag, London, 1989).
30. J. G. GRASELLI, M. K. SNAVELY and B. J. BULKIN, *Phys. Reports* **65** (1980) 231.
31. L. N. OVANDER, *Opt. Spectrosc.* **9** (1960) 302.
32. R. LOUDON, *Adv. Phys.* **13** (1964) 423.
33. *Idem.*, *ibid.* **14** (1965) 621.
34. R.-J. ROE, *J. Appl. Phys.* **36** (1965) 2024.
35. S. P. S. PORTO, *J. Opt. Soc. Am.* **56** (1966) 1585.
36. J. R. SCHERER, S. KINT and G. F. BAILEY, *J. Mol. Spectrosc.* **39** (1971) 146.
37. C. V. RAMAN and K. S. KRISHNAN, *Nature* **122** (1928) 169.
38. R. G. SNYDER, *J. Mol. Spectrosc.* **37** (1971) 353.
39. D. I. BOWER, *J. Phys. B: Atom. Mol. Phys.* **9** (1976) 3275.
40. D. I. BOWER, *J. Polym. Sci.: Polym. Phys. Ed.* **19** (1981) 93.
41. S. NOMURA, N. NAKAMURA and H. KAWAI, *J. Polym. Sci.: Part A-2* **9** (1971) 407.
42. B. J. BERNE, P. PECHUKAS and G. D. HARP, *J. Chem. Phys.* **49** (1968) 3125.
43. H. POTTTEL, W. HERREMAN, B. W. VAN DER MEER and M. AMELOOT, *Chem. Phys.* **102** (1986) 37.
44. F. L. LABARTHET, T. BUFFETEAU and C. SOURISSEAU, *Appl. Spectrosc.* **54** (2000) 699.
45. D. I. BOWER, *Polym.* **23** (1982) 1251.
46. D. I. BOWER, D. A. JARVIS and I. M. WARD, *J. Polym. Sci.: Part B: Polym. Phys.* **24** (1986) 1459.
47. N. E. SCHLOTTER and J. F. RABOLT, *Polym.* **25** (1984) 165.
48. G. Y. NIKOLAEVA, L. E. SEMENOVA, K. A. PROKHOROV and S. A. GORDEYEV, *Laser Phys.* **7** (1997) 403.
49. G. Y. NIKOLAEVA, L. E. SEMENOVA, K. A. PROKHOROV and S. A. GORDEYEV, *Opt. Spectrosc.* **85** (1998) 416.
50. K. PROKHOROV, S. GORDEYEV, G. NIKOLAEVA, P. PASHININ, R. WITHNALL, I. DUNKIN and S. SHILTON, *Macromol. Symp.* **184** (2002) 123.
51. I. W. SHEPHERD, in "Chapter 4: Raman Polarization Techniques in the Study of Macromolecules", in "Advances in Infrared and Raman Spectroscopy", edited by R. E. HESTER and R. J. H. CLARK (Heyden & Son, London, 1977).
52. J. STOKR, B. SCHNEIDER, D. DOSKOILOVA, J. LOVY and P. SEDLACEK, *Polym.* **23** (1982) 714.
53. S. JEN, N. A. CLARK, P. S. PERSHAN and E. B. PRIESTLEY, *Phys. Rev. Lett.* **31** (1973) 1552.
54. S. MICHIELSEN, "Application of Raman Spectroscopy to Organic Fibers and Films" in "Handbook of Raman Spectroscopy", edited by I. R. LEWIS and H. G. M. EDWARDS (Marcel Dekker, New York, 2001).
55. N. J. EVERALL, *Appl. Spectrosc.* **52** (1998) 1498.
56. T. C. DAMEN, S. P. S. PORTO and B. TELL, *Phys. Rev.* **142** (1966) 570.

40TH ANNIVERSARY

57. E. HECHT, in "Optics" (Addison-Wesley, Reading, 1987).
58. H. C. VAN DE HULST, in "Light Scattering by Small Particles" (Dover, New York, 1981).
59. L. D. CAMBON, J. L. RAMONJA and D. V. LUU, *J. Raman Spectrosc.* **18** (1987) 129.
60. S. YANG and S. MICHIELSEN, *Macromolecules* **35** (2002) 10108.
61. R. J. ROE and W. R. KRIGBAUM, *J. Appl. Phys.* **35** (1964) 2215.
62. R.-J. ROE and W. R. KRIGBAUM, *J. Chem. Phys.* **40** (1964) 2608.
63. S. K. FREEMAN, in "Applications of Laser Raman Spectroscopy" (John Wiley & Sons, London, 1973).
64. I. M. WARD, in "Structure and Properties of Oriented Polymers, 2nd Ed." (Chapman & Hall, London, 1997).
65. C.-P. LAFRANCE, P. CHABOT, M. PIGEON, R. E. PRUD'HOMME and M. PEZOLET, *Polym.* **34** (1993) 5029.
66. C. C. LESKO, J. F. RABOLT, R. M. IKEDA, B. CHASE and A. KENNEDY, *J. Mol. Struct.* **521** (2000) 127.
67. P. R. MORRIS, *J. Appl. Phys.* **40** (1969) 447.
68. P. H. HERMANS, in "Physics and Chemistry of Cellulose Fibres -with particular Reference to Rayon" (Elsevier Publishing Company, Inc., New York, 1949).
69. W. J. JONES, D. K. THOMAS, D. W. THOMAS and G. WILLIAMS, *J. Mol. Struct.* **614** (2002) 75.
70. V. B. GUPTA and S. KUMAR, *J. Polym. Sci.: Polym. Phys. Ed.* **17** (1979) 1307.
71. E. L. V. LEWIS, D. I. BOWER and I. M. WARD, *Polym.* **36** (1995) 4741.
72. R. T. BAILEY, A. J. HYDE and J. J. KIM, *Spectrochim. Acta* **30A** (1974) 91.
73. M. J. GALL, P. J. HENDRA, C. J. PEACOCK, M. E. A. CUDBY and H. A. WILLIS, *Spectrochim. Acta* **28A** (1972) 1485.
74. M. PIGEON, R. E. PRUD'HOMME and M. PEZOLET, *Macromolecules* **24** (1991) 5687.
75. I. W. SHEPHERD, in "Chapter 4: Raman Polarization Techniques in the Study of Macromolecules", in "Advances in Infrared and Raman Spectroscopy Vol. 3," edited by R. E. Hester, R. J. H. Clark (Heyden, London, 1977).
76. N. EVERALL, K. DAVIS, H. OWEN, M. J. PELLETIER and J. SLATER, *Appl. Spectrosc.* **50** (1996) 388.
77. S. P. S. PORTO, J. A. GIORDMAINE and T. C. DAMEN, *Phys. Rev.* **147** (1966) 608.
78. D. I. BOWER and I. M. WARD, *Polym.* **23** (1982) 645.
79. J. MAXFIELD, R. S. STEIN and M. C. CHEN, *J. Polym. Sci.: Polym. Phys. Ed.* **16** (1978) 37.
80. J. PURVIS and D. I. BOWER, *J. Polym. Sci.: Polym. Phys. Ed.* **14** (1976) 1461.
81. J. PURVIS and D. I. BOWER, *Polym.* **15** (1974) 645.
82. W. T. WILSER and D. B. FITCHEN, *J. Chem. Phys.* **62** (1975) 720.
83. P. D. VASKO and J. L. KOENIG, *Macromolecules* **3** (1970) 597.
84. N. EVERALL, H. OWEN and J. SLATER, *Appl. Spectrosc.* **49** (1995) 610.
85. M. A. DE BAEZ, P. J. HENDRA and M. JUDKINS, *Spectrochim. Acta* **A51** (1995) 2117.
86. S. JEN, N. A. CLARK, P. S. PERSHAN and E. B. PRIESTLEY, *J. Chem. Phys.* **66** (1977) 4635.
87. W. T. WILSER and D. B. FITCHEN, *Biopolymers* **13** (1974) 1435.
88. J. L. DEROUAULT, P. J. HENDRA, M. E. A. CUDBY and H. A. WILLIS, *J. Chem. Soc., Chem. Comm.* (1972) 1187.
89. B. FANCONI, B. TOMLINSON, L. A. NAFIE, W. SMALL and W. L. PETICOLAS, *J. Chem. Phys.* **51** (1969) 3993.
90. E. L. V. LEWIS and D. I. BOWER, *J. Raman Spectrosc.* **18** (1987) 61.
91. G. TURRELL, C. BREMARD, P. DHAMELINCOURT and J. LAUREYNS, *Appl. Spectrosc.* **39** (1985) 1036.
92. R. E. PRUD'HOMME, L. BOURLAND, R. T. NATARAJAN and R. S. STEIN, *J. Polym. Sci., Polym. Phys. Ed.* **12** (1974) 1955.
93. M. J. CITRA, D. B. CHASE, R. M. IKEDA and K. H. GARDNER, *Macromolecules* **28** (1995) 4007.
94. C. BREMARD, P. DHAMELINCOURT, J. LAUREYNS and G. TURRELL, *J. Mol. Struct.* **142** (1986) 13.
95. M. E. ANDERSEN and R. Z. MUGGLI, *Anal. Chem.* **53** (1981) 1772.
96. F. ADAR and H. NOETHER, *Polym.* **26** (1985) 1935.
97. G. TURRELL and J. CORSET (Ed.), in "Raman Microscopy Development and Applications" (Harcourt Brace & Company, London, 1996).
98. G. TURRELL, *J. Raman Spectrosc.* **15** (1984) 103.
99. C. BREMARD, J. LAUREYNS and G. TURRELL, *Can. J. Spectrosc.* **32** (1987) 70.
100. B. JASSE and J. L. KOENIG, *J. Polym. Sci.: Polym. Phys. Ed.* **18** (1980) 731.
101. J. A. TOPP and W. KLEFER, *Appl. Spectrosc.* **28** (1974) 26.
102. W. F. MADDAMS, *Spectrochim. Acta* **50A** (1994) 1967.
103. B. H. STUART, *Vib. Spectrosc.* **10** (1996) 79.
104. K. MIYANO, *J. Chem. Phys.* **69** (1978) 4807.
105. C.-P. LAFRANCE, P. CHABOT, M. PIGEON, R. E. PRUD'HOMME and M. PEZOLET, *Polym.* **34** (1993) 5029.
106. S. LU, A. E. RUSSELL and P. J. HENDRA, *J. Mater. Sci.* **33** (1998) 4721.
107. J. PURVIS, D. I. BOWER and I. M. WARD, *Polym.* **14** (1973) 398.
108. F. J. BOERIO and R. A. BAILEY, *Polym. Lett. Ed.* **12** (1974) 433.
109. J. C. RODRIGUEZ-CABELLO, J. C. MERINO, L. QUINTANILLA and J. M. PASTOR, *J. Appl. Polym. Sci.* **62** (1996) 1953.
110. S. NATARAJAN and S. MICHIELSEN, *J. Appl. Polym. Sci.* **73** (1999) 943.
111. R. A. HUIJTS and S. M. PETERS, *Polym.* **35** (1994) 3119.
112. S. YANG and S. MICHIELSEN, *Macromolecules* **36** (2003) 6484.
113. S. YANG and S. MICHIELSEN, *J. Polym. Sci.: Part B: Polym. Phys.* **42** (2004) 47.
114. N. EVERALL, P. TAYLER, J. M. CHALMERS, D. MCKERRON, R. FERWERDA and J. H. VAN DER MAAS, *Polym.* **35** (1994) 3184.
115. N. J. EVERALL, J. LUMSDON, J. M. CHALMERS and N. MASON, *Spectrochim. Acta* **47A** (1991) 1305.
116. P. J. HENDRA and T. R. GILSON (Ed.), "Laser Raman Spectroscopy" (Wiley, London, 1970) Chap.7.
117. S. FRISK, R. M. IKEDA, D. B. CHASE, A. KENNEDY and J. F. RABOLT, *Macromolecules* **37** (2004) 6027.
118. A. S. NIELSEN and R. PYRZ, *Composites Sci. Technol.* **62** (2002) 2219.
119. N. EVERALL, J. CHALMERS and P. MILLS, *Appl. Spectrosc.* **50** (1996) 1229.
120. R. J. SAMUELS, *J. Polym. Sci.: Part A 3* (1965) 1741.
121. I. KARACAN, A. K. TARAIYA, D. I. BOWER and I. M. WARD, *Polym.* **34** (1993) 2691.
122. J. M. PASTOR, T. JAWHARI, J. C. MERINO and J. FRAILE, *Makromol. Chem., Macromol. Symp.* **72** (1993) 131.
123. C. H. WANG and D. B. CAVANAUGH, *J. Appl. Phys.* **52** (1981) 6003.
124. X. WANG and S. MICHIELSEN, *J. Appl. Polym. Sci.* **82** (2001) 1330.
125. D. GARCIA-LOPEZ, J. C. MERINO and J. M. PASTOR, *ibid.* **88** (2003) 947.

126. H. DOSHI, S. KUMAR, M. SRINIVASRAO, J. O. PARK and D. A. SCHIRALDI, *Polym.* **43** (2002) 1701.
127. M. R. FERNANDEZ, J. C. MERINO, M. I. GOBERNADO-MITRE and J. M. PASTOR, *Appl. Spectrosc.* **54** (2000) 1105.
128. A. R. BHATTACHARYA, T. V. SREEKUMAR, T. LIU, S. KUMAR, K. M. ERICSON, R. H. HAUGE and R. E. SMALLEY, *Polym.* **44** (2003) 2373.
129. M. J. FOLKES, M. KASHIWAGI and I. M. WARD, *ibid.* **12** (1971) 697.
130. B. JASSE, R. S. CHAO and J. L. KOENIG, *J. Polym. Sci.: Polym. Phys. Ed.* **16** (1978) 2157.
131. J. F. RABOLT and B. FANCONI, *Macromolecules* **11** (1978) 740.
132. K. ZABEL, N. E. SCHLOTTER and J. F. RABOLT, *Macromolecules* **16** (1983) 446.
133. P. B. SMITH, A. LEUGERS, S. KANG, X. YANG and S. L. HSU, *Macromol. Symp.* **175** (2001) 81.
134. P. B. SMITH, A. LEUGERS, S. KANG, S. L. HSU and X. YANG, *J. Appl. Polym. Sci.* **82** (2001) 2497.
135. H. TAKEUCHI, M. MATSUNO, S. A. OVERMAN and G. J. THOMAS JR, *J. Am. Chem. Soc.* **118** (1996) 3498.
136. M. TSUBOI, S. A. OVERMAN and G. J. THOMAS, JR, *Biochemistry* **35** (1996) 10403.
137. M. TSUBOI, M. SUZUKI, S. A. OVERMAN and G. J. THOMAS, JR, *Biochemistry* **39** (2000) 2677.
138. M.-E. ROUSSEAU, T. LEFEVRE, L. BEAULIEU, T. ASAKURA and M. PEZOLET, *Biomacromolecules* **5** (2004) 2247.
139. S.-H. LEE and S. KRIMM, *J. Raman Spectrosc.* **29** (1998) 73.
140. S. A. OVERMAN, M. TSUBOI and G. J. THOMAS, JR, *J. Mol. Biol.* **259** (1996) 331.
141. W.-Y. YEH and R. J. YOUNG, *J. Macromol. Sci.-Phys.* **B37** (1998) 83.
142. S. KOUTEVA-ARGUIROVA, W. SEIFERT, M. KITTLER and J. REIF, *Mater. Sci. Eng.* **B102** (2003) 37.
143. V. B. GUPTA, S. K. SATT and D. D. DEORUKHKAR, *Polym. Comm.* **30** (1989) 341.
144. S. K. BAHL, D. D. CORNELL, F. J. BOERIO and G. E. MCGRAW, *Polym. Lett. Ed.* **12** (1974) 13.
145. C. W. BUNN, R. P. DAUBENY and C. J. BROWN, *Proc. Roy. Soc. Lond.* **A226** (1955) 531.
146. I. M. WARD, *Proc. Phys. Soc.* **80** (1962) 1176.
147. I. M. WARD, in "Mechanical Properties of Solid Polymers, 2nd ed." (John Wiley & Sons, Chichester, 1983).
148. A. REUSS, *Zeit. Angew. Math. Mech.* **9** (1929) 49.
149. T. NISHINO, K. NAKAMAE, F. YOKOYAMA and T. MATSUMOTO, *J. Macromol. Sci.-Phys.* **B27** (1988) 407.
150. K. KAJI and I. SAKURADA, *Makromol. Chem., Suppl.* **1** (1975) 599.
151. C. E. SHANNON, *Bell Sys. Tech. J.* **27** (1948) 379.
152. C. E. SHANNON and W. WEAVER, in "Mathematical Theory of Communication" (University of Illinois Press, Urbana Illinois, 1949).
153. A. H. W. BECK, in "Statistical Mechanics, Fluctuations, and Noise" (Edward Arnold, London, 1976).
154. E. T. JAYNES, in "Information Theory and Statistical Mechanics", in "Statistical Physics", edited by K. W. FORD (W. A. Benjamin Inc., New York, 1963).
155. E. S. R. GOPAL, in "Statistical Mechanics and Properties of Matter Theory and Applications" (Ellis Horwood Limited, Chichester, 1974).